Association of Oxo−Molybdenum Dithiolene Complexes with a Multiamide Additive and Its Influence on the Ease of O-Atom Transfer

Hiroyuki Oku, Norikazu Ueyama, and Akira Nakamura*

Department of Macromolecular Science, Faculty of Science, Osaka University, Toyonaka, Osaka 560, Japan

Received October 2, 1995[⊗]

To regulate the reactivity of dithiolene dioxomolybdenum(VI) complexes, two systems were studied: (1) chelate recognition with a diamide additive, 1,3-bis(isobutyrylamino)benzene (**1**); (2) a dithiolene complex with four amide substituents, $(n\text{-}Pr_4N)_2[Mo^{IV}O\{S_2C_2(CONH_2)_2\}_2]\cdot 0.5(i\text{-}PrOH)\cdot DMF$ (**2**) ($S_2C_2(CONH_2)_2$ = 1,2-dicarbamoylethylene-1,2-dithiolate). Both amide compounds, the additive **1** and the complex **2**, were designed to form NH···S and/or NH···O hydrogen bonding with thiolate ligands in $(Mo^{VI}O_2)^{2+}$ and $(Mo^{IV}O)^{2+}$ complexes. Titration analyses indicate the presence of a 1:1 complex in CH_2Cl_2 solution. This association causes changes in solubility and reactivity of the molybdenum complexes. When the additive was mixed with a DMSO-d_6 solution of $(NEt_4)_2[Mo^{IV}O\{S_2C_2(COOMe)_2\}_2]$ (**3**) ($S_2C_2(COOMe)_2$ = 1,2-di(methoxycarbonyl)ethylene-1,2-dithiolate), the rate of reduction of Me_3NO was increased by a factor of 6. An acceleration was also observed for compound **2**. It appears that NH···S hydogen bonding is modulating the system.

Introduction

The regulation of enzymatic reactivity occurs widely in living organisms and is utilized to control the rate of various metabolic processes.[1] The regulation is sometimes done by allosteric enzymes[1,2] where signal compounds act as activators or inhibitors.

To study the regulation of a biomimetic reaction, we have employed model compounds of metalloenzymes, especially of the molybdenum oxidoreductases.[3] Generally, the latter mediate the oxo transfer reaction in the respiratory chain and in small molecule metabolism via O-atom transfer between Mo(VI) and Mo(IV) oxidation states.[4] The metal center is surrounded by a number of thiolate ligands[5,6] that include the pterin cofactor.[7] The pterin cofactor is a dithiolene ligand involving phosphate and pterin substituents. Resonance Raman,[8] variable temperature MCD,[9] and crystallography[6b] of dimethyl sulfoxide (DMSO) reductase have suggested the bis-coordination of the dithiolate to Mo(IV) and Mo(VI) centers. A similar type of coordination seems to be involved in the metal center of other molybdenum oxidoreductases that contain the pterin cofactor.

In the molybdenum enzyme active site, we have proposed[10,11] the involvement of molecular devices, such as NH···S hydrogen bond formation, in the regulation of the oxo transfer reaction. Actually, the presence of NH···S hydrogen bonds has been found at most of the active centers of electron transfer proteins, such as iron−sulfur proteins[12] and blue copper proteins[13] in which the NH···S hydrogen bond regulates the metal−thiolate bonding.[14,15a] In model systems, NH···S hydrogen bonds has been shown to be one of the important factors for the positive shifts of the redox potentials of reduced rubredoxin peptide model complexes, especially in nonpolar solvent, e.g., $[Fe^{II}(Z\text{-}\mathbf{cys}\text{ProLeu}\mathbf{cys}\text{GlyVal-OMe})_2]^{2-}$.[14] Simple hydrogen-bonded model systems containing metal thiolates, e.g., Mo(V) and Mo(IV),[15] Cu(II),[16] Fe(II) and Co(II),[17] and iron−sulfur ($[Fe_4S_4]^{2+}$ and $[Fe_2S_2]^{2+}$)[18] have also been reported. Therefore, we intended to modulate metal−thiolate bonding with an appropriate molecular association system between a model compound and an amide additive as described below.

[⊗] Abstract published in *Advance ACS Abstracts*, February 15, 1997.

(1) Dixon, M.; Webb, E. C. *Enzymes*; Longman: London, 1979. Cohen, P. *Control of enzyme activity*; Chapman and Hall: London, 1976.
(2) Monod, J.; Changeux, J.-P.; Jacob, F. *J. Mol. Biol.* **1963**, *6*, 306.
(3) (a) Young, C. G.; Wedd, A. G. In *Encyclopedia of Inorganic Chemistry*; King, R. B., Ed.; John Wiley & Sons: Chichester, U.K., 1994; Vol. 5, p 2320. (b) Pilato, R. S.; Stiefel, E. I. In *Bioinorganic Catalysis*; Reedijk, J., Ed.; Marcel Dekker, Inc.: New York, 1993; p 131. (c) Enemark, J. H.; Young, C. G. *Adv. Inorg. Chem.* **1993**, *40*, 1. (d) Wootton, J. C.; Nicolson, R. E.; Cock, J. M.; Walters, D. E.; Burke, J. F.; Doyle, W. E.; Bray, R. C. *Biochem. Biophys. Acta* **1991**, *1057*, 157.
(4) Holm, R. H. *Chem. Rev.* **1987**, *87*, 1401.
(5) George, G. N.; Garrett, R. M.; Prince, R. C.; Rajagoparan, K. V. *J. Am. Chem. Soc.* **1996**, *118*, 8588.
(6) (a) Chan, M. K.; Mukund, S.; Kletzin, A.; Adams, M. W. W.; Rees, D. C. *Science* **1995**, *267*, 1463. (b) Schindelin, H.; Kisker, C.; Hilton, J.; Rajagopalan, K. V.; Rees, D. C. *Science* **1996**, *272*, 1615. (c) Romao, M. J.; Archer, M.; Moura, I.; Moura, J. J. G.; LeGall, J.; Engh, R.; Schneider, M.; Hof, P.; Huber, R. *Science* **1995**, *270*, 331. (d) Huber, R.; Hof, P.; Duarte, R. O.; Moura, J. J. G.; Moura, I.; Liu, M.-Y.; LeGall, J.; Hille, R.; Archer, M.; Romão, M. J. *Proc. Natl. Acad. Sci. U.S.A.* **1996**, *93*, 8846.
(7) (a) Johnson, J. L.; Bastian, N. R.; Rajagopalan, K. V. *Proc. Natl. Acad. Sci. U.S.A.* **1990**, *87*, 3190. (b) Bastian, N. R.; Kay, C. J.; Barber, M. J.; Rajagopalan, K. V. *J. Biol. Chem.* **1991**, *266*, 45.
(8) Gruber, S.; Kilpatrick, L.; Bastian, N. R.; Rajagopalan, K. V.; Spiro, T. G. *J. Am. Chem. Soc.* **1990**, *112*, 8180.
(9) (a) Benson, N.; Farrar, J. A.; McEwan, A. G.; Thomson, A. J. *FEBS Lett.* **1992**, *307*, 169. (b) Finnegan, M. G.; Hilton, J.; Rajagopalan, K. V.; Johnson, M. K. *Inorg. Chem.* **1993**, *32*, 2616.
(10) Oku, H.; Ueyama, N.; Nakamura, A. *Inorg. Chem.* **1995**, *34*, 3667.
(11) Oku, H.; Ueyama, N.; Nakamura, A. Submitted for publication.
(12) (a) Adman, E. T. *Adv. Protein Chem.* **1991**, *42*, 145. (b) Adman, E.; Watenpaugh, K.; Jensen, L. H. *Proc. Natl. Acad. Sci. U.S.A.* **1975**, *72*, 4954. (c) Tsukihara, T.; Fukuyama, K.; Nakamura, M.; Katsube, Y.; Kanaka, N.; Kakudo, M.; Hase, T.; Wada, K.; Matsubara, H. *J. Biochem. (Tokyo)* **1979**, *90*, 1763. (d) Watenpaugh, K. D.; Sieker, L. C.; Jensen, L. H. *J. Mol. Biol.* **1979**, *131*, 509.
(13) Baker, E. N. *J. Mol. Biol.* **1988**, *203*, 1071.
(14) Nakamura, A.; Ueyama, N. *Adv. Inorg. Chem.* **1989**, *33*, 39. (b) Ueyama, N.; Terakawa, T.; Nakata, M.; Nakamura, A. *J. Am. Chem. Soc.* **1983**, *105*, 7098. (c) Ohno, R.; Ueyama, N.; Nakamura, A. *Inorg. Chem.* **1991**, *30*, 4887. (d) Sun, W. Y.; Ueyama, N; Nakamura, A. *Inorg. Chem.* **1993**, *32*, 1095. (e) Sun, W. Y. Ph.D. Thesis, Osaka University, 1993. (f) Sun, W. Y.; Ueyama, N.; Nakamura, A. *Inorg. Chem.* **1991**, *30*, 4026. (g) Sun, W. Y.; Ueyama, N.; Nakamura, A. *Inorg. Chem.* **1992**, *31*, 4053.
(15) (a) Ueyama, N.; Okamura, T.; Nakamura, A. *J. Am. Chem. Soc.* **1992**, *114*, 8129. (b) Huang, J.; Ostrander, R. L.; Rheingold, A. L.; Leung, Y.; Walters, M. A. *J. Am. Chem. Soc.* **1994**, *116*, 6769.
(16) Okamura, T.; Ueyama, N.; Nakamura, N.; Ainscough, E. W.; Brodie, A. M.; Waters, J. M. *J. Chem. Soc., Chem. Commun.* **1993**, 1658.

S0020-1669(95)01277-8 CCC: $14.00

Previously, we reported two systems which model the O-atom transfer reaction (eq 1).[10,19] The systems contain $(NEt_4)_2[Mo^{IV}O\{S_2C_2(COOMe)_2\}_2]$ (**3**)[20] or $(PPh_4)_2[Mo^{IV}O\{S_2C_2(CN)\}_2]$ (**4**)[19,21] and Me_3NO.

$$[Mo^{IV}O(S_2C_2R_2)_2]^{2-} + Me_3NO \rightarrow [Mo^{VI}O_2(S_2C_2R_2)_2]^{2-} + Me_3N \quad (1)$$

(R = COOMe or CN)

To accelerate the O-atom transfer reaction in eq 1, we have designed two hydrogen-bonding systems. One is a multiamide additive, 1,3-bis(isobutyrylamino)benzene (=$(i\text{-PrCONH})_2C_6H_4$) (**1**) which can preferentially interact with two thiolate sulfur atoms via its two amide NH groups. The other is an amide modified dithiolene complex, $(n\text{-Pr}_4N)_2[Mo^{IV}O\{S_2C_2(CONH_2)_2\}_2]\cdot 0.5(i\text{-PrOH})\cdot$DMF (**2**), which has two primary amide groups on the dithiolene ligand for NH···S (thiolate) and NH···O (amide carbonyl) interactions.

In this paper, the regulation of reductive reactivity of molybdenum(IV) complexes **2**−**4** is presented. To confirm the interaction of the dithiolene model complexes **3** and **4** with the amide additive, **1**, ^{1}H NMR, cyclic voltammetry, and vibrational spectroscopy were utilized.

Experimental Section

All operations were carried out under argon atmosphere. *N*,*N*-Dimethylformamide (DMF), diethyl ether, 2-propanol (*i*-PrOH), dichloromethane, acetonitrile, dimethoxyethane, and dimethyl-d_6 sulfoxide (DMSO-d_6) were purified by distillation before use.

Materials. The persulfide complex, $(n\text{-Pr}_4N)_2[Mo^{IV}O(S_4)_2]\cdot i$-PrOH (**5**), was prepared by the modified method of the reported procedure for the corresponding Et_4N^+ salt by Coucouvanis et al.[20] Anal. Calcd for $C_{27}H_{64}O_2N_2MoS_8$: C, 40.47; H, 8.05; N, 3.50. Found: C, 40.26; H, 7.94; N, 3.96. IR (KBr): 927 cm^{-1} (ν(Mo═O)). $(NEt_4)_2[Mo^{IV}O\{S_2C_2(COOMe)_2\}_2]$ (**3**), $(PPh_4)_2[Mo^{IV}O\{S_2C_2(CN)_2\}_2]$ (**4**), and $(PPh_4)_2[Mo^{VI}O_2\{S_2C_2(CN)_2\}_2]\cdot$2MeOH (**6**) were prepared by the reported procedures.[20,21] The Me_3NO used was of commercial grade.

2,6-Bis(isobutyrylamino)benzene (=$(i\text{-PrCONH})_2C_6H_4$) (1). To 300 mL of dimethoxyethane was added *m*-phenylenediamine (5.0 g, 46 mmol), following isobutyryl chloride (9.9 g, 92 mmol) at 0 °C and triethylamine (15 mL, 130 mmol). After being stirred for 2 h, the solution was allowed to stand at room temperature with continued mixing for 12 h. The mixture was filtered, and the solution obtained was extracted with 70 mL of ethyl acetate twice. The separated ether layer was washed with 50 mL of a 3% $NaHCO_3$ aqueous solution twice and with 50 mL of NaCl-saturated aqueous solution three times, successively. The solution was dried over anhydrous magnesium sulfate and concentrated under reduced pressure to give white powder which was recrystallized from hot CH_3CN; yield, 514 mg (22%). ^{1}H NMR (CD_2Cl_2): δ 1.21 (12H, CH_3), 2.47 (2H, CH), 7.25 (3H, $-H_{3,4,5}$), 7.89 (1H, $-H_1$). Anal. Calcd for $C_{14}H_{20}N_2O_2$: C, 67.72; H, 8.12; N, 11.28. Found: C, 67.81; H, 8.19; N, 11.03.

Synthesis of $(n\text{-Pr}_4N)_2[Mo^{IV}O\{S_2C_2(CONH_2)_2\}_2]\cdot 0.5(i\text{-PrOH})\cdot$DMF (2). The synthesis of titled compound was carried out under argon atmosphere. The persulfide complex, **5** (880 mg, 1.19 mmol), and acetylenedicarboxamide (**7**)[22] (270 mg, 2.41 mmol) were dissolved in DMF (5 mL). When the mixture stood at 50 °C, the color of the solution changed from pale brown to dark brown within 10 min. Colorless solid was precipitated during stirring at room temperature for 12 h. The mixture was filtered, and tetrahydrofuran (THF) (2 mL) was added. Red prismatic crystals and yellow powder were formed, when stored at −20 °C. The crystals were collected; yield, 5 mg (<1%). Hygroscopic. ^{1}H NMR (DMF-d_7): δ 6.74 (brs, $-NH_2$). Anal. Calcd for $C_{32}H_{64}O_5N_6MoS_4$ (crystallized solvent was removed by evacuation): C, 45.91; H, 7.71; N, 10.04. Found: C, 44.69; H, 7.50; N, 9.54.

Molecular Modeling. Molecular dynamics and molecular orbital calculations were performed on SGI Indigo2 and Power indigo2 workstations using Cerius2 (Moleular Simulation, 1993 and 1995) and SPARTAN (Wavefunction Inc., 1993 and 1995) software packages, respectively.

The molecular dynamics calculation for dithiolene complexes and the multiamide additive was performed with UNIVERSAL force field[23] at 300 K. Due to the limitation of the force field which does not include hydrogen bonding terms, only "electrostatic" and "van der Waals" terms can contribute to form intermolecular interactions (e.g., NH···S bondings). Due to the lack of a hydrogen bonding term, the additive was moving away and did not keep interacting with any functional group of the dithiolene complexes during the dynamics simulation. Therefore, we have used the molecular orbital calculation to estimate association structures.

Physical Measurements. ^{1}H NMR NOESY spectra were recorded on Varian Unity Plus 600 and JEOL GSX-400 spectrometers in CD_2Cl_2 at 30 °C. The solution IR spectra were recorded on a Jasco FT/IR-8300 spectrometer at 25 ± 1 °C in CH_2Cl_2 (conditions: 0.1 mm cell length (KBr), 2 cm^{-1} resolution, 800 scans). Raman spectra were taken on Jasco R-800, NR-1800, and Bio-Rad FT Raman spectrophotometers equipped with a HTV-R649 photomultiplier and liquid N_2 cooled CCD and InGaAs detectors, respectively, at 25 ± 1 °C. Exciting radiation was provided by He−Ne (632.8 nm (∼2 mW)), Ar (514.5 and 457.9 nm (1∼3 mW)), or Nd:YAG laser (1064 nm, 380 mW). In the case of photomultiplier detection, wavenumbers of the Raman bands are determined from the expanded spectra at each region (5 cm^{-1} slit width, 1−5 s dwell time/0.2−1.0 cm^{-1} step, 8−64 scans). In the case of CCD detection, an accumulation time was 60 s. Wavenumber calibrations were carried out with natural emissions of a neon lamp from 0−2000 cm^{-1} as the standard. In the case of FT-Raman measurement, the conditions are follows: 380 mW laser power (focused at the sample), 4 cm^{-1} resolution, 8000 scans. The UV/vis absorption spectra were recorded on a Jasco Ubest-30 with use of a 1 mm cell under argon atmosphere.

Kinetic Measurements. Reaction systems containing the monooxomolybdenum(IV) complex **4** or **2** and Me_3NO in DMF were monitored spectrophotometrically in the region 250−900 nm. A typical measurement was carried out using a 1 mm UV cell containing a solution of monooxomolybdenum(IV) complex (1 mM) at 27 °C. After thermal equilibrium, a Me_3NO solution (ca. 100 mM, also at 27 °C) was injected through a silicone rubber cap and the cell contents were quickly mixed by shaking. For the reaction of **4**, the time dependence of the absorbance for dioxomolybdenum(VI) was measured every 30 min and the data analysis was performed by absorbance at 420 nm (O and S → Mo^{VI} charge transfer band).

For complex **3**, the oxidation reaction with Me_3NO in DMSO-d_6 at 27 °C was monitored using a 270 MHz ^{1}H NMR spectrometer (JEOL EX-270) with measurements of the ^{1}H signals of methoxy groups in dioxomolybdenum(VI) complex **3**. A solution of Me_3NO (100 mM) in a 5 mm NMR gastight tube containing the monooxomolybdenum(IV) complex solution (ca. 1 mM) was prepared under argon atmosphere, and the contents were quickly mixed by shaking at 27 °C. The ^{1}H NMR spectra were taken every 30 or 60 min.

Crystallographic Data Collections and Data Reduction of 2. The diffraction data were collected on a Rigaku AFC-7R equipped with graphite monochromated Mo Kα radiation. The unit cell parameters

(17) (a) Walters, M. A.; Dewan, J. C.; Min, C.; Pinto, S. *Inorg. Chem.* **1991**, *30*, 2656. (b) Ueyama, N.; Okamura, T.; Nakamura, A. *J. Chem. Soc., Chem. Commun.* **1992**, 1019. (c) Ueyama, N.; Nishikawa, N.; Yamada, Y.; Okamura, T.; Nakamura, A. *J. Am. Chem. Soc.* **1996**, *118*, 12826.

(18) Ueyama, N.; Kimura, S.; Yamada, Y.; Okamura, T.; Nakamura, A. *Inorg. Chem.* **1996**, *35*, 6473.

(19) Oku, H.; Ueyama, N.; Nakamura, A.; Kai, Y.; Kanehisa, N. *Chem. Lett.* **1994**, 607.

(20) Coucouvanis, D.; Hadjikyriacou, A.; Toupadakis, A.; Koo, S.; Ileperuma, O.; Draganjac, M.; Salifoglou, A. *Inorg. Chem.* **1991**, *30*, 754.

(21) Different procedure for the syntheses of $[Mo^{IV}O\{S_2C_2(CN)_2\}_2]^{2-}$ and $[Mo^{VI}O_2\{S_2C_2(CN)_2\}_2]^{2-}$ have been reported respectively by: McCleverty, J. A.; Locke, J.; Ratcliff, B.; Wharton, E. *Inorg. Chim. Acta* **1964**, *3*, 283. Das, S. K.; Chaudhury, P. K.; Biswas, D.; Sarkar, S. *J. Am. Chem. Soc.* **1994**, *116*, 9061.

(22) Saggiomo, A. J. *J. Org. Chem.* **1957**, *22*, 1171.

(23) (a) Casewit, C. J.; Colwell, K. S.; Rappe, A. K. *J. Am. Chem. Soc.* **1992**, *114*, 10046. (b) Rappe, A. K.; Casewit, C. J.; Colwell, K. S.; Goddard, W. A., III; Skiff, W. M. *J. Am. Chem. Soc.* **1992**, *114*, 10024. (c) Casewit, C. J.; Colwell, K. S.; Rappe, A. K. *J. Am. Chem. Soc* **1992**, *114*, 10035. (d) Allured, V. S.; Kelly, C. M.; Landis, C. R. *J. Am. Chem. Soc.* **1991**, *113*, 1.

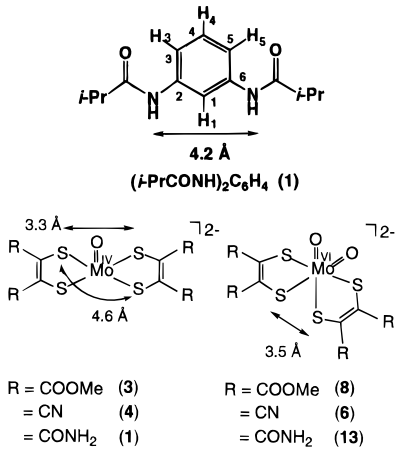

Figure 1. Structural diagrams of the multiamide additive (*i*-PrCONH)$_2$C$_6$H$_4$ (**1**) and dithiolene complexes (NEt$_4$)$_2$[Mo^{IV}O{S$_2$C$_2$(COOMe)$_2$}$_2$] (**3**), (NEt$_4$)$_2$[Mo^{VI}O$_2$\{S$_2$C$_2$(COOMe)$_2$\}$_2$] (**8**), (*n*-Pr$_4$N)$_2$[Mo^{IV}O\{S$_2$C$_2$(CONH$_2$)$_2$\}$_2$]·0.5(*i*-PrOH)·DMF (**2**), (PPh$_4$)$_2$[Mo^{IV}O\{S$_2$C$_2$(CN)$_2$\}$_2$] (**4**), (PPh$_4$)$_2$[Mo^{VI}O$_2$\{S$_2$C$_2$(CN)$_2$\}$_2$]·2MeOH (**6**), and (*n*-Pr$_4$N)$_2$[Mo^{VI}O$_2$\{S$_2$C$_2$(CONH$_2$)$_2$\}$_2$] (**13**).

were determined and refined from setting angles of 25 accurately centered reflections. Data were collected with the ω scan method. Three standard reflections were measured every 100 reflections and revealed no fluctuations in intensities. The data were corrected for Lorentz and polarization effects. An emperical absorption correction was applied using the ψ scan method. The structure was solved by the direct methods and successive Fourier difference syntheses. The non-hydrogen atoms were refined anisotropically. Hydrogen atom coordinates were included at idealized positions with an assumed C−H, N−H, and O−H distance of 1.08, 1.01, and 0.97 Å, respectively, and not refined. The final cycles of least-squares refinement were based on 4772 observed reflections ($I > 3.00\sigma(I)$), and 534 variable parameters and converged with $R = 0.052$ and $R_w = 0.061$. Both factors are defined as $R = \sum(|F_o| - |F_c|)/\sum|F_o|$ and $R_w = [\sum w(|F_o| - |F_c|)^2/\sum w|F_o|^2]^{1/2}$. Neutral atom scattering factors and anomalous dispersion effects (the values for $\Delta f'$ and $\Delta f''$) were referenced from the International Tables for X-ray Crystallography (1974). All calculations were performed using the TEXSAN crystallographic software package of Molecular Structure Corp.

Results

Multiamide Additive, (*i*-PrCONH)$_2$C$_6$H$_4$ (1). Synthesis of the Additive, 1. The structure of the multiamide additive, **1**, is illustrated in Figure 1. Before the additive, **1**, was synthesized, this structure was checked by molecular dynamics and by molecular orbital calculations in order to satisfy the appropriate complexation geometry with the dithiolene complexes. When the two amide groups are in π-conjugation with the connected benzene ring ($C_1-C_{2,6}-N-H$ torsion angles are 180°), the distance between the two amide NH groups is minimized to 4.2 Å. On the other hand, for example, if the $C_1-C_{2,6}-N-H$ torsion angles are set to ±90°, respectively, the two amino groups will appear on the same side of the benzene plane. The distances between the two amide NH groups will then be 5.3 Å. If the two amino groups exist on the opposite side of the benzene plane, the distances between the two amide NH groups will be wider than in the case of same side orientation, although this conformation is not suitable for the chelate interaction. The available amide distances are comparable to the interligand S···S distances of **3**, **4** (*trans* S−Mo−S distance for **3** is 4.6 Å [31] and for **4** is 4.6 Å [19]) and **6** (the distance between two thiolates (coordinated at the *trans* position to oxo ligands) is 3.5 Å).

There are three reasons to employ a diamide frame, (RCONH)$_2$C$_6$H$_4$, on **1**: (1) to provide a large electrostatic interaction specifically by the two amide groups; (2) to be able to prevent the association among the additive molecules probably due to the rigid structure of (RCONH)$_2$C$_6$H$_4$; (3) to gain a significant entropy advantage (chelating effect) by the multidentate coordination of the additive over the polar solvent molecules (monodentate ligand). To realize a molecular association between the additive, **1**, and a thiolato complex, we must displace solvating molecules from the complex. Usually polar solvent molecules, such as DMSO, DMF, and CH$_3$CN, have only one interacting group, S═O, C═O, and −C≡N, respectively, as a monodentate ligand to solvate to the complex. Therefore, a multidentate ligand like, **1**, may compete successfully with solvent molecules for the complex via the chelate effect. For example, a multidentate hydrogen bonding recognition has already been proven in CD$_3$OD solution for the scorpion receptor.[24]

The skeleton of (RCONH)$_2$C$_6$H$_4$ has already been shown to have an advantage in providing a large electrostatic interaction specifically with the two thiolate ligands and carbonyl groups in the following Fe(II) and Fe(III) complexes, e.g., [Fe^{III}(S$_2$-*o*-xyl)$_2$]$^{1-}$, [Fe^{II}(S$_2$-*o*-xyl)$_2$]$^{2-}$ (S$_2$-*o*-xyl = 1,2-*o*-xylylenedithiolato) and [Fe^{II}(*Z*-**cys**ProLeu**cys**GlyVal-OMe)$_2$]$^{2-}$.[25] In this study, intermolecular NOE peaks and the positive shift of the redox potentials were observed.

Molecular Modeling for the Additive and the Dithiolene Complexes. To determine if additive **1** can interact with the dithiolene complexes, **3**, **4**, **6**, and [Mo^{VI}O$_2$\{S$_2$C$_2$(COOMe)$_2$\}$_2$]$^{2-}$ (**8**), we have performed geometry optimization through molecular orbital calculations. To minimize complexity in the calculation, we have used simplified compounds. As additive and Mo(IV) and Mo(VI) dithiolene complexes, 1,3-(formylamino)-benzene (=(HCONH)$_2$C$_6$H$_4$ (**9**)), [Mo^{IV}O(1,2-ethylenedithiolato)$_2$]$^{2-}$ (**10**), and [Mo^{VI}O$_2$(1,2-ethylenedithiolato)$_2$]$^{2-}$ (**11**) were used.

Molecular orbital calculations were carried out using semiemperical method (PM3 for transition metals[24]). Initially, the geometries of all three compounds, **9**−**11**, were optimized by the calculation. For **11**, we have observed the elongation of Mo^{VI}−S bonds (*trans* to oxo = 2.6135 Å, *cis* to oxo = 2.5211 Å). This is due to the strong π-donating effect of oxo and thiolate ligands as observed in the crystal structure of (M^{VI}O$_2$)$^{2+}$ (M = Mo and W) thiolato complexes.[19,30,37,39] Through the optimization, the heats of formation for each compound were obtained (for **9**, −44.357 kcal/mol; ($\angle$(H−N−C$_{2,6}$−C$_1$) = 0°); for **10**, 164.309 kcal/mol; and **11**, 100.518 kcal/mol). Therefore, if an associated structure has an energy at lower than 56.161 (for the **11**−**9** system) or 119.952 kcal/mol (for the **10**−**9** system), the calculated structure will gain stabilization energy, although the solvent effect cannot be included in this PM3 (for transition metals) method.

(24) Hehre, W. J.; Yu, J. G. *Abstr. Pap. Am. Chem. Soc.* **1996**, *211*, 216-PMSE. (b) Hehre, W. J.; Yu, J. G. *Abstr. Pap. Am. Chem. Soc.* **1995**, *210*, 77-COMP.
(25) Zaima, H. Thesis, Osaka University, 1994.
(26) (a) Macomber, R. S. *J. Chem. Educ.* **1992**, *69*, 375. (b) Conn, M. M.; Deslongchamps, G.; Mendoza, J. d.; Rebeck, J., Jr. *J. Am. Chem. Soc.* **1993**, *115*, 3548. (c) Connors, K. A. *Binding Constants*; John Wiley & Sons: New York, 1987.
(27) (a) Bell, R. A.; Saunders, K. A. *Can. J. Chem.* **1970**, *48*, 1114. (b) Noggle, J. H.; Schirmer, R. E. *The Nuclear Overhauser Effect-Chemical Applications*; Academic Press: New York, 1972. (c) Sanders, J. K. M.; Hunter, B. K. *Modern NMR Spectroscopy*; Oxford University Press: New York, 1987.
(28) The value in the parentheses represents the maximum error range calculated from the volume difference of two peaks in the NOESY spectrum.
(29) Morokuma, K. *Acc. Chem. Res.* **1977**, *10*, 294.
(30) Oku, H.; Ueyama, N.; Nakamura, A. *Bull. Chem. Soc. Jpn.* **1996**, *69*, 3139.
(31) (a) Randles, J. E. B. *Trans. Faraday Soc.* **1948**, *44*, 327. (b) Sevcik, A. *Collect. Czech. Chem. Commun.* **1948**, *13*, 349.
(32) Oku, H.; Ueyama, N.; Kondo, M.; Nakamura, A. *Inorg. Chem.* **1994**, *33*, 209.
(33) Coucouvanis, D.; Toupadakis, A.; Lane, J. D.; Koo, S. M.; Kim, C. G.; Hadjikyriacou, A. *J. Am. Chem. Soc.* **1991**, *113*, 5271.

Table 1. Obtained Energies (Heats of Formation, kcal/mol), Interaction Distances (Å), and H−N−$C_{2,6}$−C_1 Torsion Angles (deg) for the Optimized Structures of $[Mo^{IV}O(1,2\text{-ethylenedithiolate})_2]^{2-}$ (**10**) + $(HCONH)_2C_6H_4$ (**9**)[a]

interaction sites	energy (kcal/mol)	interaction distances (Å)		H−N−$C_{2,6}$−C_1 torsion angle (deg)
S1−S2 (Mo═O5 side on the dithiolene plane)	13.332	NH···S1	1.8385	13.8141
		NH···S2	1.8394	−13.8537
		(CH_1···O5	2.4257)	
S1−S2 (opposite side to Mo═O5 on the dithiolene plane)	20.239	NH···S1	1.8230	−0.0508
		NH···S2	2.3799	−0.0010
S1−S3 (Mo═O5 side of the dithiolene plane)	17.881	NH···S1	2.3531	14.5794
		NH···S3	2.3534	−14.5788
		(CH_1···O5	1.8677)	
S1−S3 (Opposite side to Mo═O5on the dithiolene plane)	(The NH group on S3 atom was moved to S4 atom through the geometry optimizing calculation.)			
S1−S4	14.263	NH···S1	1.8640	10.3614
		NH···S4	1.8642	10.5142
S1−O5	16.059	NH···S1	1.8266	0.9566
		NH···O5	1.8619	−6.1710
		(CH_1···O5	2.3632)	

[a]Atom numbering is shown in Figure 1 and 2.

Initial structures between the additive, (**9**) and the dithiolene complex (**10** or **11**) were constructed by using two interactions among NH···S, NH···O(oxo ligand), NH···π(dithiolene C═C), π(dithiolene C═C)···π(benzene ring), CH(benzene ring)···O-(oxo ligand), CH(benzene ring)···S, and CH(benzene ring)··· π(benzene ring) bondings. From the calculations, NH···π, π···π, and CH···π interactions were not maintained through the optimizing processes and were changed to form other favorable bondings (e.g., NH···S and CH···O). Repeated attempts to achieve those expected interactions by starting optimizations with different initial association structures were not successful. For CH···O or CH···S interaction, the minimized structures did not show lower energy compared with the NH···O or NH···S associated form. For example, in the interaction between Mo(VI) complex **11** and additive **9** the binding at NH···O(oxo ligand) and CH($H_{3,6}$ of benzene ring)···S(*cis* to Mo^{VI}═O) gave a minimized energy (heat of formation) at 89.764 kcal/mol which is higher than the other obtained energy values shown in Table 2.

Tables 1 and 2 listed all the possible binding forms using the NH···S and NH···O interactions for Mo(IV) and Mo(VI) complexes **10** and **11** with additive **9**. All associated structures showed their energy in the range of 13.332−20.239 kcal/mol (for the **10**−**9** system) or 81.252−88.787 kcal/mol (for the **11**−**9** system). Therefore, with their stabilization energy, each associated form is expected to exist in the actual system. Especially, in each system two association forms showed lower energy compared with other NH···X (X = electron donor) bound structures (for the **10**−**9** system, 13.332 and 14.263 kcal/mol; for the **11**−**9** system, 81.252 and 88.787 kcal/mol) (Figures 2 and 3).

IR and Raman Spectral Studies for the Mixtures of the Additive 1 and Each of the Dithiolene Complexes (3, 4, or 6). The formation of hydrogen bonds was directly detected by shifts in the ν(N−H) band. Figure 4 shows the ν(N−H) region of CH_2Cl_2 solution IR spectra for the additive **1** in the presence and the absence of the dithiolene complexes. The spectrum of the additive **1** contains a strong peak at 3428 cm^{-1} and a broad peak at 3330 cm^{-1}. The former band is associated with the non-hydrogen bonded NH, and the latter is to the hydrogen bonded NH. The ratio of the peak area, 90:10 (=3428 cm^{-1}: 3330 cm^{-1}) indicates the intermolecular hydrogen bond of **1** to be negligible. When the dithiolene complexes are mixed with the additive **1** a broad band due to hydrogen bonded NH around 3330 cm^{-1} was increased in intensity. Therefore, the NH group is an interaction site of the additive **1**. The ratio of the peak area, 60:40 (=3428 cm^{-1}:~3330 cm^{-1}) directly indicates the amount of association with **1**.

To determine the hydrogen bonding site, Raman and IR spectra were compared for each of the dithiolene complexes (**3**, **4**, or **6**) in the presence and the absence of **1**. The possible binding sites are on thiolato, carbonyl, and cyano groups. Unfortunately, any significant shift was not observed in band wavenumbers of ν(Mo−S), ν(Mo═O), ν(C═C), ν(C≡N), and ν(C═O). Therefore, we could not determine the hydrogen bonding site on the dithiolene complexes from the vibrational spectroscopy.

^{1}H NMR Saturation Studies for NH Signals. A saturated solution of **1** was 4 mM in CD_2Cl_2 solution but increased to 7 mM in the presence of 7 mM concentrations of **3**, **4**, or **6**, suggesting an association. Actually, ^{1}H NMR studies showed a low-field shift of the NH signals when **1** is added gradually to 7 mM solutions of each dithiolene complex **3**, **4**, or **6** (Figure 5). These titration analyses suggest the presence of a 1:1 complex. Due to the limitation of NMR sensitivity, we cannot obtain the plots at lower concentrations of **1** ([**1**] = 0.01−0.05 mM) to make association constant[26] values meaningful.

^{1}H NMR NOESY Spectra of (i-PrCONH)$_2$C$_6$H$_4$ (1) and the Mixtures of 1 with Complexes, 3, 4, and 6. NOESY spectra were taken to determine the conformation of **1** in solution. Peak volumes were calculated from the contour plot of the spectra. The conformation of **1** (Table 3 and Figure 6) provides information required for the associated structure between **1** and the thiolato complexes.

Additive (i-PrCONH)$_2$C$_6$H$_4$ (1). Figure 7 shows 600 MHz ^{1}H NMR NOESY spectra. NOEs between −CH_3 of the isopropyl group and H_1 of the benzene ring (cross peak a), and between NH and H_1 (b) were observed. For $H_{3,5}$, no cross peaks were observed with the −NH and the −CH_3 signals. In

(34) (a) Shibahara, T.; Sakane, G.; Mochida, S. *J. Am. Chem. Soc.* **1993**, *115*, 10408. (b) Rakowski DuBois, M.; VanDerveer, M. C.; DuBois, D. L.; Haltinger, R. C.; Miller, W. K. *J. Am. Chem. Soc.* **1980**, *102*, 7456. (c) Weberg, R.; Halttiwanger, R. C.; Rakowski DuBois, M. *Organometallics* **1985**, *4*, 1315. (d) Young, C. G.; Yan, X. F.; Fox, B. L.; Tiekink, E. R. T. *J. Chem. Soc., Chem. Commun.* **1994**, 2579. (e) Eagle, A. A.; Harben, S. M.; Tiekink, E. R.; Young, C. G. *J. Am. Chem. Soc.* **1994**, *116*, 9749. (f) Pilato, R. S.; Eriksen, K.; Greaney, M. A.; Stiefel, E. I.; Goswami, S.; Kilpatrick, L.; Spiro, T. G.; Taylor, E. C.; Rheingold, A. L. *J. Am. Chem. Soc.* **1991**, *113*, 9372.
(35) Kuleshova, L. N.; Zorkii, P. M. *Acta Crystallogr.* **1981**, *B37*, 1363.
(36) Kondo, M.; Oku, H.; Ueyama, N.; Nakamura, A. Submitted for publication in *Bull. Chem. Soc. Jpn.*
(37) Ueyama, N.; Oku, H.; Nakamura, A. *J. Am. Chem. Soc.* **1992**, *114*, 7310.
(38) (a) Ueyama, N.; Oku, H.; Kondo, M.; Okamura, T.; Yoshinaga, N.; Nakamura, A. *Inorg. Chem.* **1996**, *35*, 643. (b) Yoshinaga, N.; Ueyama, N.; Okamura, T.; Nakamura, A. *Chem. Lett.* **1990**, 1655.
(39) Oku, H.; Ueyama, N.; Nakamura, A. *Chem. Lett.* **1996**, 31.

Table 2. Obtained Energies (Heats of Formation, kcal/mol), Interaction Distances (Å), and H−N−$C_{2,6}$−C_1 Torsion Angles (deg) for the Optimized Structures of $[Mo^{VI}O_2$(1,2-ethylenedithiolate)$_2]^{2-}$ (**11**) + $(HCONH)_2C_6H_4$ (**9**)[a]

interaction sites	energy (kcal/mol)	interaction distances (Å)		H−N−$C_{2,6}$−C_1 torsion angles (deg)
S1−S2	81.306	NH···S1	1.8553 (*trans* to Mo═O)	8.5390
		NH···S2	1.8549 (*trans* to Mo═O)	8.2367
S1−S3 (Mo═O5 side on the dithiolene plane)	84.846	NH···S1	1.8278 (*trans* to Mo═O)	11.6772
		NH···S3	2.3195 (*cis* to Mo═O)	−14.2354
		(CH_1···O5	2.3474)	
S1−S3 (opposite side to Mo═O5 on the dithiolene plane)	86.283	NH···S1	2.3296 (*trans* to Mo═O)	−14.4348
		NH···S3	2.5222 (*cis* to Mo═O)	16.4238
S1−S4	81.252	NH···S1	1.8443 (*trans* to Mo═O)	1.6772
		NH···S4	1.8124 (*cis* to Mo═O)	−14.2354
S1−O5	85.408	NH···O3	1.8297	6.7822
		NH···S5	1.8255 (*trans* to Mo═O)	−8.2539
		(CH_1···O5	2.3376)	
S3−O5	82.371	NH···O3	1.8108	−1.0140
		NH···S5	1.8179 (*cis* to Mo═O)	−1.0514
		(CH_1···O5	2.4529)	
S3−O6	87.797	NH···O6	1.8548	−3.2778
		NH···S3	1.8334 (*cis* to Mo═O)	6.3189
		(CH_1···O5	2.6722)	
		(CH_1···O6	1.8802)	
S3−O5,O6 (NH groups were found between O5 and O6 and on S3)	83.885	NH···O5	2.5608	0.6407
		NH···O6	2.5307	3.1746
		NH···S3	1.8152 (*cis* to Mo═O)	
		(CH_1···O5	1.9047)	
		(CH_1···O6	2.4207)	
O5−O6	88.787	NH···O5	1.8353	−1.0140
		NH···O6	1.8548	−1.0514
		(C_1H···O5	2.3645)	
		(CH_1···O6	1.8421)	

[a]Atom numbering is shown in Figure 2.

this case, the C_1−$C_{2,6}$−N−H dihedral angle is estimated to be 0°. The proposed conformation of the additive **1** is shown in Figure 6a.

Mixture of 1 with $(NEt_4)_2[Mo^{IV}O\{S_2C_2(COOMe)\}_2]$ (3). In the NOESY spectra (Figure 8), cross peaks were observed for the pairs $-CH_3-H_1$ (cross peak a), $-CH_3-H_3$ (b), NH−H_1(c), and NH−$H_{3,5}$ (d). Ideally, the rate of growth of the NOE (the intensity of NOE) between two spins depends on r^{-6} (r = distance between the two spins).[27] Therefore, the H−N−$C_{2,6}$−C_1 dihedral angle can be determined by the peak volume ratio of NOEs according to the equation $(1/(R^{-1/6}+1))$, where R is the value of the peak volume ratio ([NH−H_1]/[NH−$H_{3,5}$]) as shown in Table 3. In general, this technique has a severe limitation. If there are two or more conformations, NOEs represent their equilibrium, not an actual state.[27]

In this case, the H−N−$C_{2,6}$−C_1 torsion angle is calculated to be ±85° (81−88°),[28] different from the case of the additive alone (Table 3 and Figure 9b). At this amide conformation, the distance[28] between the NH groups is 5.5 (5.4−5.5) Å (two NH are on the same side of the additive benzene ring) or 5.8 (5.7−5.8) Å (two NH are on the opposite side of the additive benzene ring) which is possible, but slightly wider to fit to the interligand S···S (=4.6 Å) structure.[20]

The conformational change of amide arms in the additive, **1**, seems to be induced by the formation of an electrostatic interaction, such as NH···X hydrogen bonds, between the NH groups on **1** and complex **3**. The interaction on sulfur atoms (NH···S hydrogen bond) is expected by the molecular orbital calculation where the HOMO of **2** is mainly dominated by thiolate pπ orbitals. The hydrogen bonding is produced by HOMO−LUMO interactions.[29]

Mixture of 1 with $(PPh_4)_2[Mo^{IV}O\{S_2C_2(CN)\}_2]$ (4). Figure 9 shows the NOESY spectrum of the mixture. The NOEs for the pairs of $H_{3,5}$−NH (cross peak a) and H_1−NH (b) were observed. From the peak volumes, the deduced torsion angle[28] of H−N−$C_{2,6}$−C_1 is ±75.3° (75.2−75.5°) (Table 3 and Figure 6c). From this dihedral angle, the distance[28] between the amide NH groups is deduced to be 5.32 (5.32−5.32) Å (two NH are on the same side of the benzene ring in **1**) or 5.60 (5.60−5.60) Å (two NH are on the opposite side of the benzene ring in **1**), which is wider than the intraligand S···S distance, 4.6 Å.[19] The conformational change of the additive **1** was also observed to be the same as that observed in the system of **1** and **3**. Interestingly, an intermolecular NOE was observed between the PPh_4^+ cation (at $H_{3,5}$) and $-CH_3$ (c). This is also evidence for the molecular association of **4** with **1**.

Mixture of 1 with $(PPh_4)_2[Mo^{VI}O_2\{S_2C_2(CN)\}_2]$ (6). From Figure 10, the NOEs were observed only for the pair of H_1−NH (cross peak a) and not for the pair of H_1-CH_3. In this case, the H−N−$C_{2,6}$−C_1 dihedral angle is estimated to be 0°. The disappearance of H_1-CH_3 NOE indicates the freezing of the conformation angle of O═C−C−H in the *i*-PrCONH− group at almost 180° as illustrated in Figure 6d. If the O═C−C−H dihedral angle is set at 180°, two CH_3- groups of *i*-Pr− will move away from a NH group. This steric vacancy around the NH groups caused by the rotation of O═C−C−H dihedral angle can make a suitable conformation of **1** in the chelate binding between two NH groups of **1** and two thiolates (*trans* to oxo) of **6**, where dithiolene ligands of **2** do not show any van der Waals contact with the CH_3- groups of **1**.

From the molecular orbital calculation, the HOMO of **6** is mainly dominated by thiolate pπ orbitals.[10,30] Therefore, the association with NH···S interaction caused by HOMO−LUMO interaction[29] can be expected as described in Figure 2 and Table 2.

In the above section, we have calculated conformation angles ($\angle$(H−N−$C_{2,6}$−C_1)) of additive **9** theoretically. Compared with spectroscopically obtained values, the Mo(IV) system (**3**−**1** and **4**−**1**, ±85° (81−88°) and ±75.3° (75.2−75.5°), respectively) did not correspond to the theoretical values (in Table 1, e.g., the lowest and second lowest energy forms of the Mo(IV) system **10**−**9** are ±12° (10−14°)). On the other hand, the Mo(VI) system (**6**−**1**, 0°) showed a close value to the theoretical values of the Mo(VI) system **11**−**9** (in Table 2, e.g., the lowest

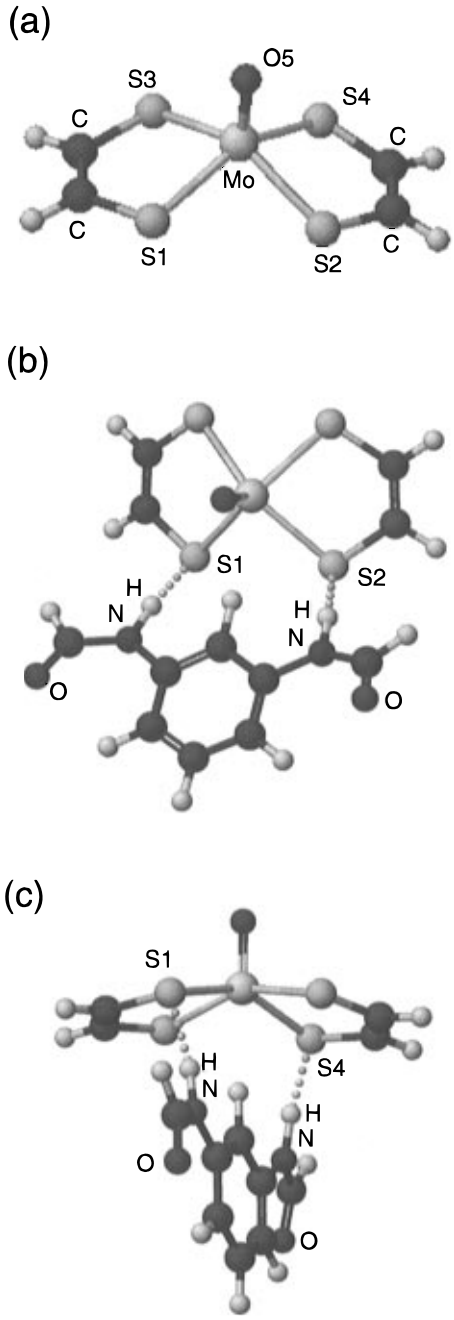

Figure 2. PM3 optimized structure for (a) $[Mo^{IV}O(1,2\text{-ethanedithiolato})_2]^{2-}$ (**10**) and the associated forms with the additive $(HCONH)_2C_6H_4$ (**9**), which have (b) the lowest (13.332 kcal/mol) and (c) the second lowest energies (14.263 kcal/mol).

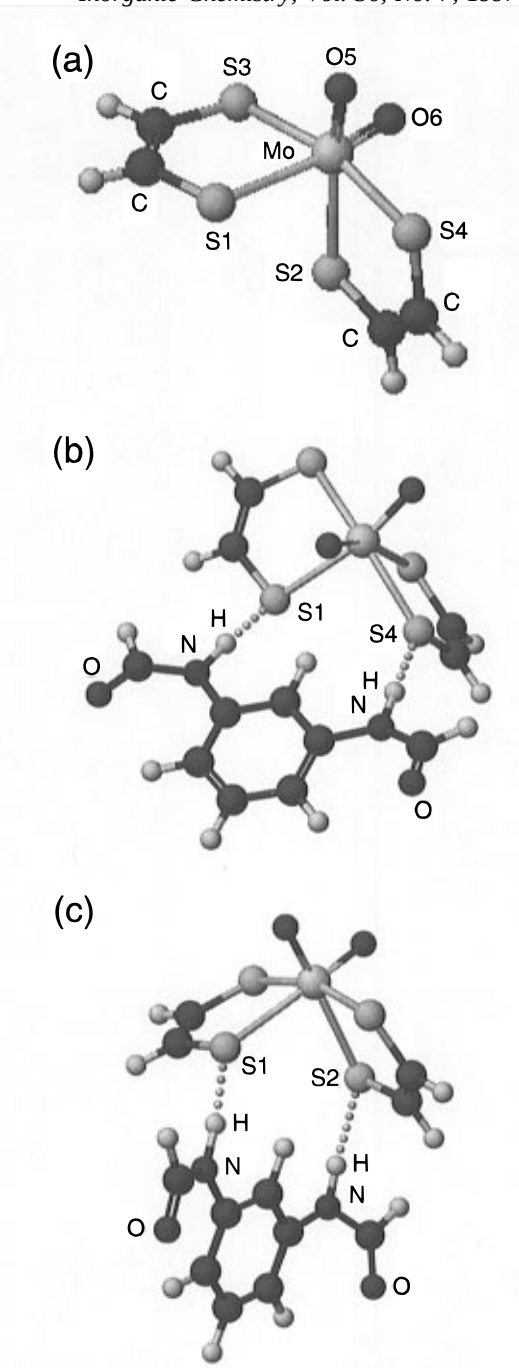

Figure 3. PM3 optimized structure of $[Mo^{VI}O_2(1,2\text{-ethanedithiolato})_2]^{2-}$ (**11**) and the associated forms with the additive $(HCONH)_2C_6H_4$ (**9**), which have (b) the lowest (81.252 kcal/mol) and (c) the second lowest energies (81.306 kcal/mol).

and the second lowest energy forms are ±2−14°). One explanation for the differences between the calculation and the observation are the lack of other interacting groups such as countercations (PPh_4^+ and NEt_4^+), −C≡N, and −COOMe, which can give other binding forms with the additive molecule in the actual system.

Electrochemical Measurements of Dithiolene Complexes 3 and 4 in the Presence of the Additive (*i*-PrCONH)$_2$C$_6$H$_4$ (1). Figure 11 shows the cyclic voltammograms of the mixture of **3** and **1** in CH_2Cl_2 at 21 °C. The oxomolybdenum(IV) dithiolene complexes **3** and **4** each show a chemically reversible Mo(V)/Mo(IV) redox process around 0 to +0.5 V (vs SCE). The electrochemical data are summarized in Table 4. The 1:1 addition of **1** resulted in a 0.065 V smaller ΔE_p value ($\Delta E_p = E_{pa} - E_{pc}$, E_{pa} and E_{pc} = anodic and cathodic peak potentials, respectively) and 70 μA larger peak current values (I_{pa}(anodic) and I_{pc}(cathodic)) with almost the same (+0.009 V positive shift) midpoint redox potential ($E_{1/2}$). The shift of E_{pa}, E_{pc}, I_{pa}, and I_{pc} values suggests faster (larger I_p values) and a more reversible (smaller ΔE_p values) electron transfer reaction at an electrode. In this case, the additive **1** probably works as a redox mediator between the complex and the electrode. If electron transfer is not accelerated by the interaction of **1** and **3**, I_p values will be smaller due to the Randles and Sevcik equation[31] ($I_p \propto D^{1/2}$), where the decrease of the diffusion constant (D) of **2** by the addition of **1** requires a decrease of the I_p values. In all measurements as shown in Table 4, the decrease of I_p was not observed.

In DMSO solvent, the 1:1 mixture of **3** and **1** showed a +0.011 V smaller ΔE_p value compared with that of complex **3** alone. This is the same trend as that observed in the CH_2Cl_2 solution. The $E_{1/2}$ value was slightly shifted to the positive side ($\Delta E_{1/2} = +0.036$ V). The observed shift of E_{pa} and E_{pc} suggests that the interaction between **1** and **3** still exists in the strongly

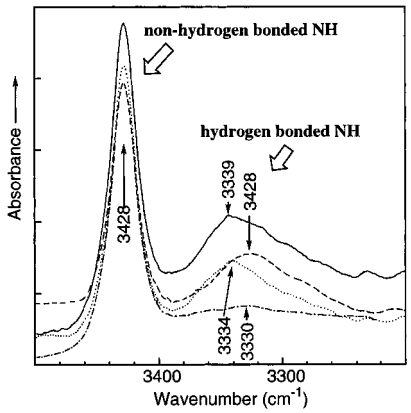

Figure 4. ν(N−H) region of IR spectra for (*i*-PrCONH)$_2$C$_6$H$_4$ (**1**) (− · −), (PPh$_4$)$_2$[Mo^{VI}O$_2${S$_2$C$_2$(CN)$_2$}$_2$]·2MeOH (**6**) + **1** (···), (PPh$_4$)$_2$-[Mo^{IV}O{S$_2$C$_2$(CN)$_2$}$_2$] (**4**) + **1** (—), and (NEt$_4$)$_2$[Mo^{IV}O{S$_2$C$_2$-(COOMe)$_2$}$_2$] (**3**) + **1** (- -) in CH_2Cl_2 at 23 °C. [Mo] = 7 mM, [**1**] = 7 mM.

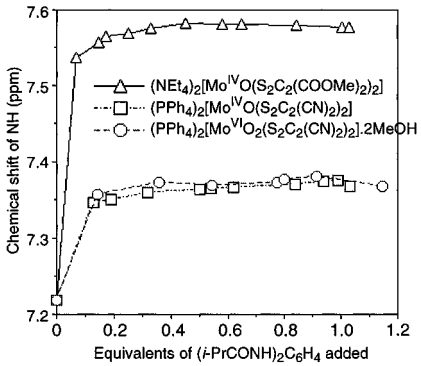

Figure 5. ^{1}H NMR saturation plot of (*i*-PrCONH)$_2$C$_6$H$_4$ (**1**) in the presence of (−△−) (NEt$_4$)$_2$[Mo^{IV}O{S$_2$C$_2$(COOMe)$_2$}$_2$] (**3**) complex, (− · −□) with (PPh$_4$)$_2$[Mo^{IV}O{S$_2$C$_2$(CN)$_2$}$_2$] (**4**), and (- -○) with (PPh$_4$)$_2$[Mo^{VI}O$_2${S$_2$C$_2$(CN)$_2$}$_2$]·2MeOH (**6**). [Mo] = 7 mM in CD_2Cl_2 at 30 °C.

Table 3. Peak Volume Ratios of NOE and the Deduced Torsion Angles (deg) of H−N−$C_{2,6}$−C_1 in (*i*-PrCONH)$_2$C$_6$H$_4$ (**1**) and (NEt$_4$)$_2$[Mo^{IV}O{S$_2$C$_2$(COOMe)$_2$}$_2$] (**3**), (PPh$_4$)$_2$[Mo^{IV}O{S$_2$C$_2$(CN)$_2$}$_2$] (**4**), and (PPh$_4$)$_2$[Mo^{VI}O$_2${S$_2$C$_2$(CN)$_2$}$_2$] (**6**) in the Presence of **1** (in CH_2Cl_2, [Mo] = 7 mM, [**1**] = 7 mM at 30 °C)

	peak volume ratio of NOE [NH ↔ H1]/[NH ↔ H3,5]	deduced torsion angle[a] for H−N−$C_{2,6}$−C_1
3 + **1**	(66 ± 6)/(34 ± 11)[b]	± 85 (81−88)
4 + **1**	(87.8 ± 0.2)/(12.2 ± 0.2)[b]	± 75.3 (75.2−75.5)
6 + **1**	100/0[c]	0
1	100/0[c]	0

[a] The value in the parentheses represents the maximum error range calculated from the volume difference of two peaks in the NOESY spectrum. [b] The experimental error range is calculated from the volume difference of two peaks (the peak shape unsymmetry in the NOESY spectrum). [c] The absence of NOEs was confirmed also by the peak volume ratio of [−CH_3 ↔ H1]/[−CH_3 ↔ H3,5], which gives the same information for the amide conformation.

polarized solvent DMSO, which is considered as a breaker of electrostatic and hydrogen bond interactions. The interaction in such a strong donor solvent is probably allowed from the multiamide structure in additive **1**, which has been made to increase the binding constant by the chelate effect.

For (PPh$_4$)$_2$[Mo^{IV}O{S$_2$C$_2$(CN)$_2$}$_2$] complex (**4**) in CH_3CN solution, the addition of **1** showed a 0.073 V smaller ΔE_p. The value of $E_{1/2}$ shifted slightly but not significantly (−0.585 → −0.536 V). Therefore, in the case of complex **4** almost the same electrochemical behavior was observed compared with that of **3**, although the redox couple did not appear in CH_2Cl_2 and DMF.

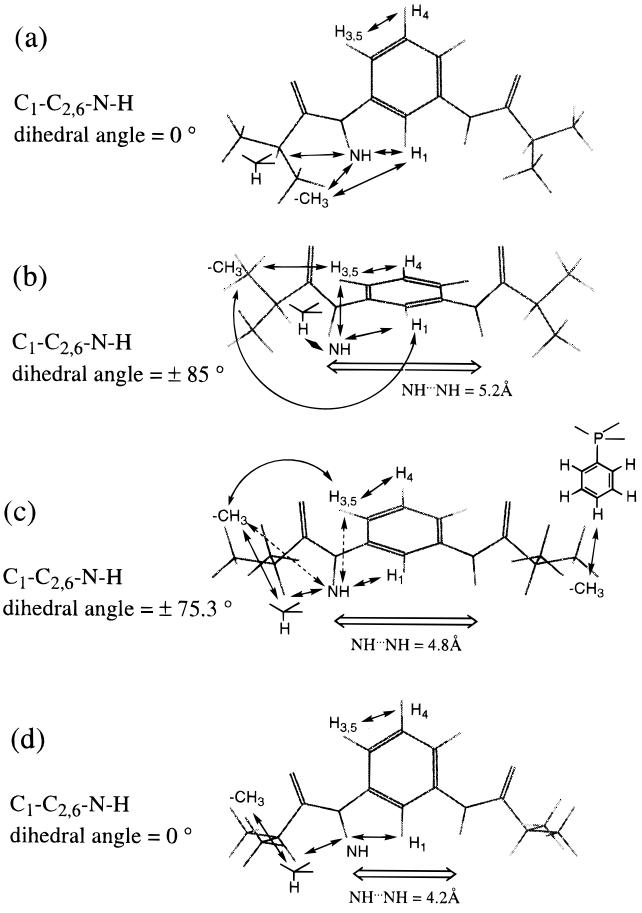

Figure 6. Map of observed NOE and the proposed conformation for (*i*-PrCONH)$_2$C$_6$H$_4$ (**1**): (a) without complex; (b) with (NEt$_4$)$_2$[Mo^{IV}O-{S$_2$C$_2$(COOMe)$_2$}$_2$] (**3**); (c) with (PPh$_4$)$_2$[Mo^{IV}O{S$_2$C$_2$(CN)$_2$}$_2$] (**4**); (d) with (PPh$_4$)$_2$[Mo^{VI}O$_2${S$_2$C$_2$(CN)$_2$}$_2$]·2MeOH (**6**). For b and c, only one of two possible conformations was shown with the equivalent orientation of two amide arms on **1**.

In conclusion, the observed smaller ΔE_p and larger I_p indicate a smooth (higher reaction rate) and reversible one electron transfer between the monooxomolybdenum(IV) dithiolene complex (**3** or **4**) and the electrode. These electrochemical changes also serve as evidence for the molecular association of complexes **3** and **4** with additive **1**.

Me$_3$NO Reduction by Dithiolene Complexes 3 and 4 in the Presence of the Additive (*i*-PrCONH)$_2$C$_6$H$_4$ (1). The spectroscopic course of the reactions of **3** and **4** with Me_3NO at the ratio $[Mo]_0$:$[Me_3NO]_0$ = 1:10 was recorded by ^{1}H NMR spectra (for **3**) and UV/vis spectra (for **4**). In the previous study,[10,19] we reported the *in situ* detection of [Mo^{VI}O$_2${S$_2$C$_2$-(COOMe)$_2$}$_2$]$^{2+}$ (**8**) by ^{1}H NMR and resonance Raman spectroscopies and the isolation of [Mo^{VI}O$_2${S$_2$C$_2$(CN)$_2$}$_2$]$^{2+}$ (**6**). The Me_3NO reduction was found to be clean and seems to follow eq 2 as observed previously for some benzenedithiolato complexes.[32]

$$(Mo^{IV}O)^{2+}\ (\mathbf{a}) + Me_3NO \rightleftharpoons [(Mo^{IV}O)^{2+}\cdot(Me_3NO)]\ (\mathbf{b}) \rightarrow (Mo^{VI}O_2)^{2+}\ (\mathbf{c}) + Me_3N \qquad (2)$$

The proposed mechanism involves the reversible coordination of Me_3NO to a vacant site of the $(Mo^{IV}O)^{2+}$ complex (**a** in eq 2) to give an intermediate, $[(Mo^{IV}O)^{2+}\cdot(Me_3NO)]$ (**b** in eq 2). Ligand rearrangement from the *trans*-$[(Mo^{IV}O)^{2+}\cdot(Me_3NO)]$ (**b**) to the *cis*- and dissociation of Me_3N give the O-atom transfer product, *cis*-$(Mo^{VI}O_2)^{2+}$ complex (**c** in eq 2).

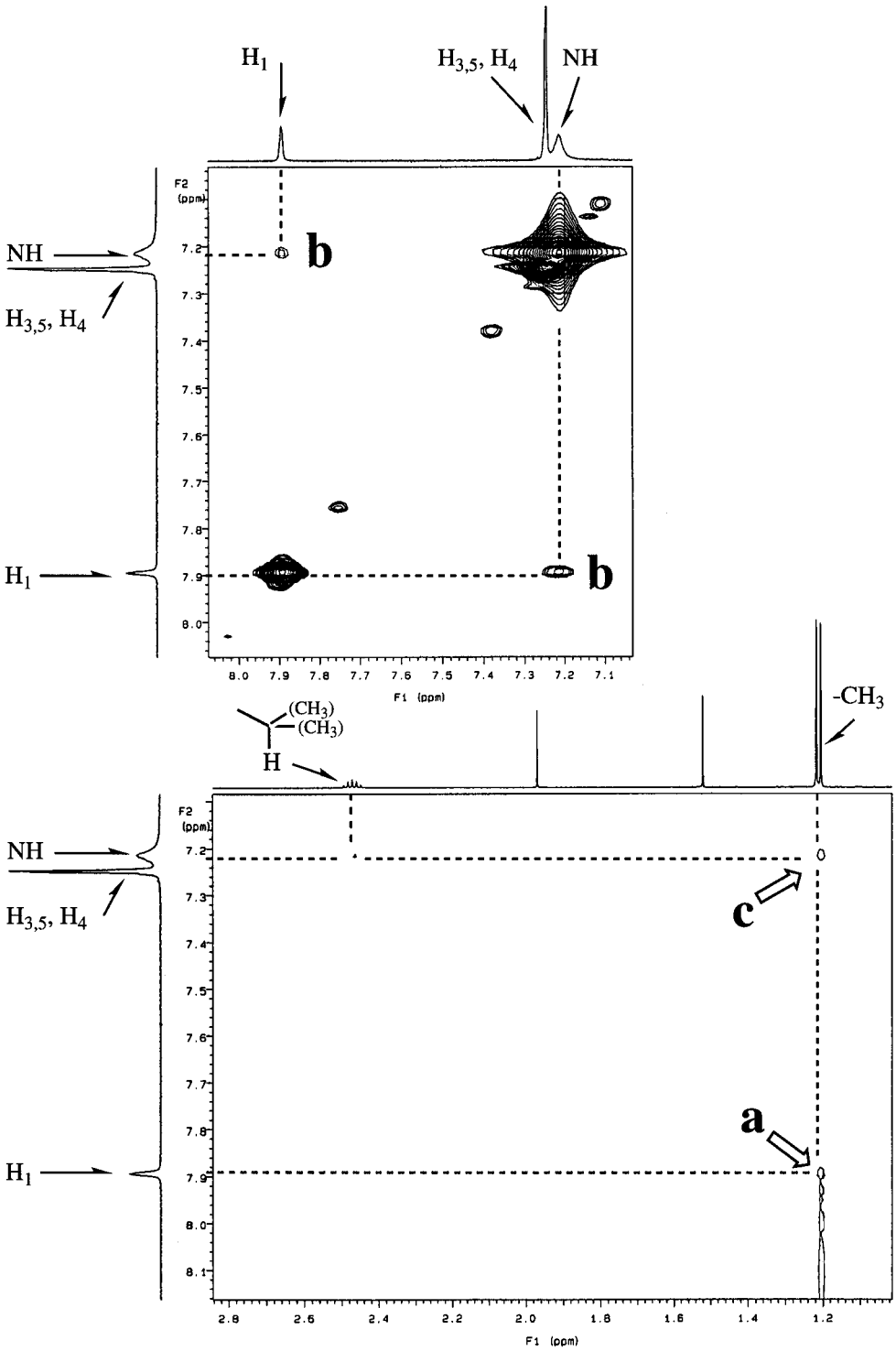

Figure 7. 600 MHz ^{1}H NMR NOESY spectra of (*i*-PrCONH)$_2$C$_6$H$_4$ (**1**) ([**1**] = 7 mM in CD_2Cl_2 at 30 °C).

Figure 12 shows time conversion curves for the reaction of **3** and the reaction of a mixture of **3** and **1**, based on ^{1}H NMR spectra. Both of the curves did not obey *pseudo*-first order kinetic behavior, even with the 10-fold excess of Me_3NO. Table 5 lists the initial reaction rates and the yield of $(Mo^{VI}O_2)^{2+}$ complex, **8**. The obtained reaction rates and the time-conversion curves clearly indicate the acceleration of Me_3NO reduction when **1** is present in the system. The observed rate enhancement in the Me_3NO reduction by the addition of **1** is explained by the acceleration of the rate of Me_3NO coordination (**a** → **b**).

On the other hand, no acceleration was observed for $S_2C_2(CN)_2$ complex **4** (Figure 13 and Table 5). In this case, the reaction obeyed pseudo-first order kinetics, where the second process (**b** → **c**) is rate determining. The rate constant slightly decreases from (11.6 ± 0.5) × 10^{-5} (for **4**) to (9.0 ± 0.3) × 10^{-5} s^{-1} (for a 1:1 mixture of **4** and **1**).

(*n*-Pr$_4$N)$_2$[Mo^{IV}O{S$_2$C$_2$(CONH$_2$)$_2$}$_2$]·0.5(*i*-PrOH)·DMF (2). To obtain evidence for the reaction acceleration by NH···S hydrogen bonding, amide groups were introduced into the dithiolene complex.

Synthetic Studies. Amide-substituted dithiolene complex **2** was prepared from the reaction of the persulfide complex **5** with acetylenedicarboxamide, **7** (eq 3). The addition reaction to

$$[Mo^{IV}O(S_4)_2]^{2-} + 2RC{\equiv}CR \rightarrow [Mo^{IV}O(S_2C_2R_2)_2]^{2-} + 0.5S_8 \quad (3)$$

polysulfides usually requires strong electrophiles such as bis-

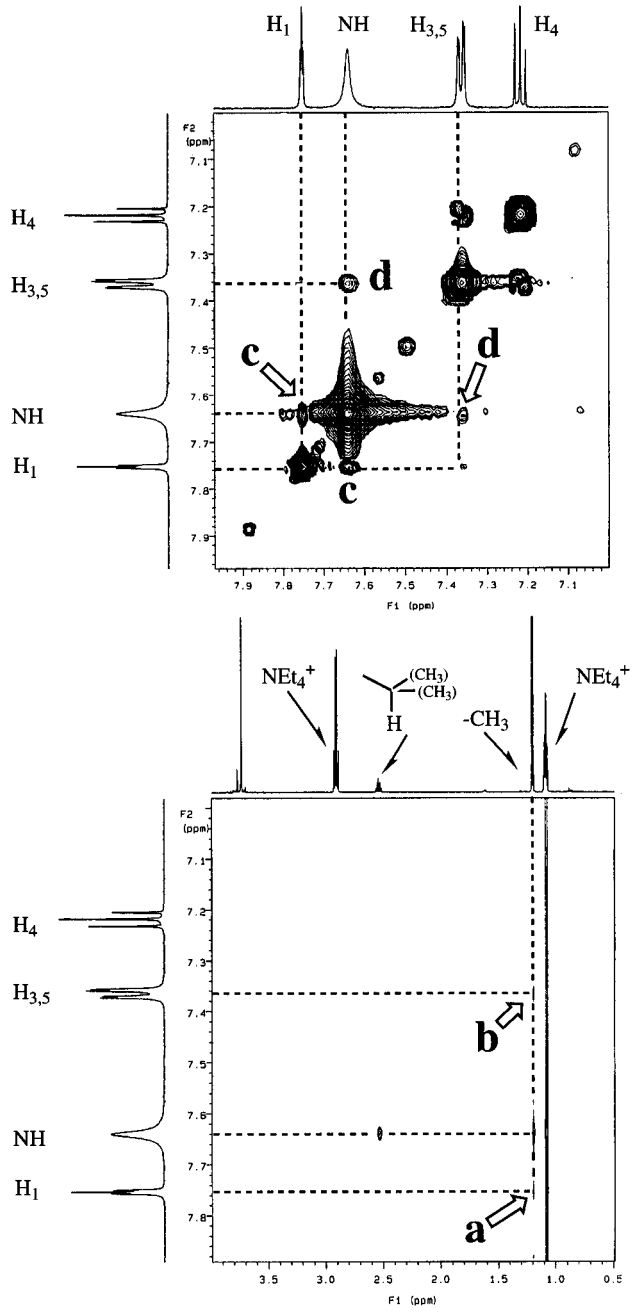

Figure 8. 600 MHz ^{1}H NMR NOESY spectra of (*i*-PrCONH)$_2$C$_6$H$_4$ (**1**) in the presence of (NEt$_4$)$_2$[Mo^{IV}O{S$_2$C$_2$(COOMe)$_2$}$_2$] (**3**) ([**1**], [**3**] = 7 mM in CD_2Cl_2 at 30 °C).

(methoxycarbonyl)acetylene (**12**).[20,33] In other cases, many actylenes, such as HC≡CH, PhC≡CPh, and $CF_3C{\equiv}CCF_3$, have been reported to add to sulfide complexes of transition metals.[34]

We have measured the frequencies of ν(C≡C) by Raman spectroscopy to acertain the electrophilicity of **7** (2236 cm^{-1}, in solid state) compared with that of **12** (2245 cm^{-1}, in liquid state). Both frequencies are higher than those of phenylacetylene (2100−2115 cm^{-1}). Therefore, we can expect enough reactivity for **7** as compared to that observed in **12**. This is probably the reason why **7** can form dithiolene complex **2** in this case.

Crystal Structure of 2. Figure 14 shows an ORTEP drawing of the anion part of **2**. Table 6 summarizes crystal and refinement data for **2**. Countercations, the complex anion, and solvent molecules (*i*-PrOH and DMF) are well-separated from each other. The Mo^{IV}OS$_4$ core of **2** has an approximately square-pyramidal geometry (C_{2v} symmetry). This structure is

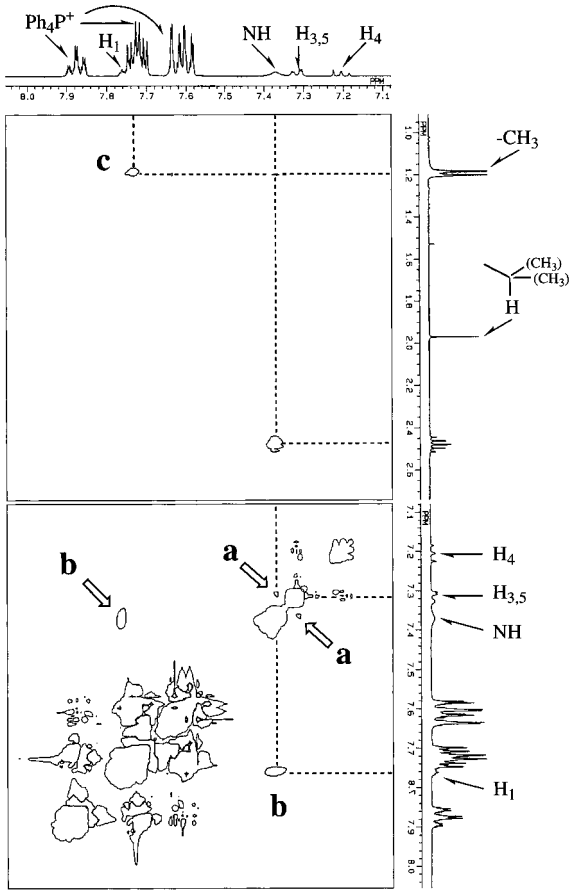

Figure 9. 400 MHz ^{1}H NMR NOESY spectra of (*i*-PrCONH)$_2$C$_6$H$_4$ (**1**) in the presence of (PPh$_4$)$_2$[Mo^{IV}O{S$_2$C$_2$(CN)$_2$}$_2$] (**4**) ([**1**], [**4**] = 7 mM in CD_2Cl_2 at 30 °C).

common to all dithiolate coordinated (Mo^{IV}O)$^{2+}$ complexes. A crystalline solvent, *i*-PrOH, was forced to locate on a C_2 axis.

For an amide group connected at C12, three different conformations were resolved on the difference Fourier map and refined for their occupancies. The identification of C and N were done by the comparison of bond lengths except for the amide group on C22. Table 7 shows the refined results of two possible conformers. From the comparison of *R* values as well as GOF values, we have choosen model 1 as an actual conformer in this crystal structure.

From the structure refinement of **2**, all NH$_2$ groups were found to be subjected to NH···S(thiolate) or NH···O(carbonyl) hydrogen bondings. All bond lenghs of NH···O and NH···S are in the range of known values.[35]

In Table 8, the selected bond angles and bond lengths are shown. Comparing the Mo−S bond lengths and Mo−S−C bond angles, we saw a larger covalency of the Mo−S bond of **2** (wider Mo−S−C angle (Δ(**2**−**4**) = 1.8°) and shorter Mo−S bond length (Δ(**2**−**4**) = 0.030 Å)) than the case of **4** due to the difference in the electronic effect of primary amide and cyano groups. In the comparison of **2** and **3**, wider Mo−S−C angles of **2** were observed than those of **3** (Δ(**2**−**3**) = 1.6° (mean)).

Raman (IR) Spectra and the Redox Potential of 2. Table 9 summarizes the bands in vibrational spectra as well as the absorption maxima of electronic spectra and redox potentials. The frequencies of ν(Mo^{IV}═O) (=915 cm^{-1}) and ν(C═C) (=1540 cm^{-1}) in **2** were almost the same as those in **3** (905 and 1535 cm^{-1}, respectively). A larger Mo−S covalency in **2** compared with that for **4** was deduced from the higher wavenumber of ν(Mo^{IV}−S) (Δ(**2**−**4**) = 23 cm^{-1}).

Four ν(N−H) bands of amide groups were observed in the IR spectra (Figure 15). These are assignable as hydrogen-

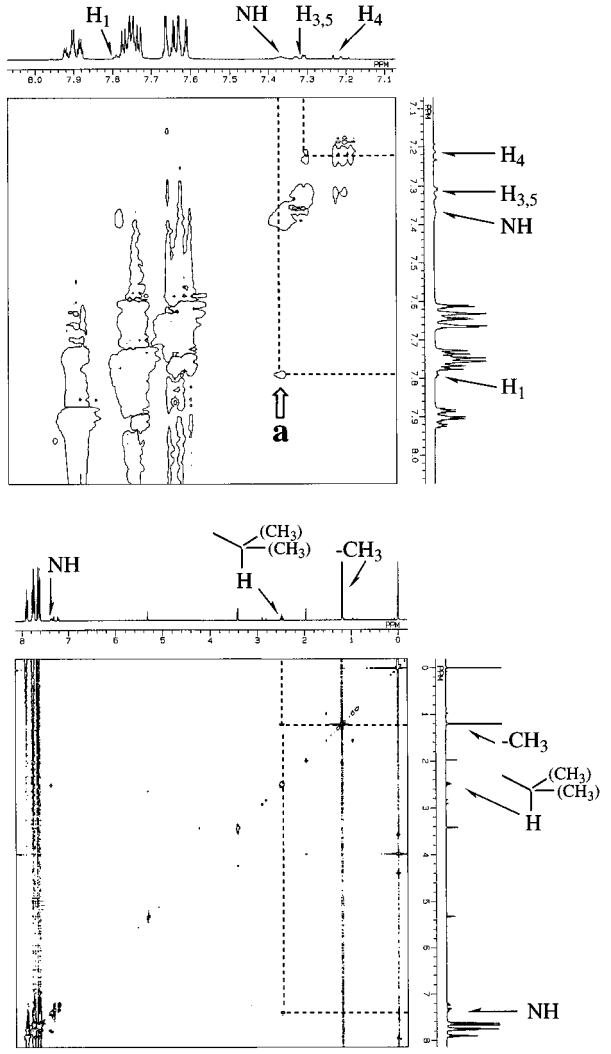

Figure 10. 400 MHz ^{1}H NMR NOESY spectra of $(i\text{-PrCONH})_2C_6H_4$ (**1**) in the presence of $(PPh_4)_2[Mo^{VI}O_2\{S_2C_2(CN)_2\}_2]\cdot 2MeOH$ (**6**) ([**1**] and [**6**] = 7 mM in CD_2Cl_2 at 30 °C)

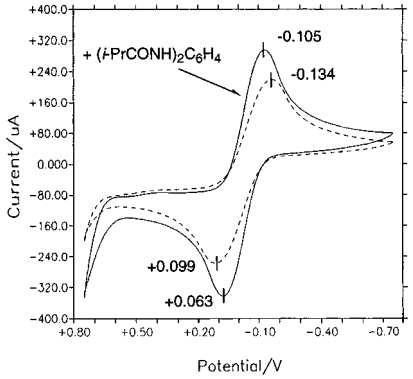

Figure 11. Cyclic voltamograms (volts vs SCE; scan rate = 100 mVs^{-1}) of $(NEt_4)_2[Mo^{IV}O\{S_2C_2(COOMe)_2\}_2]$ (**3**) (7 mM) in the presence of $(i\text{-PrCONH})_2C_6H_4$ (**1**) (1:1 (=mol/mol)) (—) and the absence of **1** (- -) in CH_2Cl_2 at 21 °C.

bonded ν(N−H) (3270(ν_{as}) and 3181(ν_s) cm^{-1}) and non-hydrogen-bonded ν(N−H) (3445(ν_{as}) and 3325(ν_s) cm^{-1}). The ratio of peak area, ∼50:∼50 (=hydrogen-bonded and non-hydrogen-bonded), indicates that half of the NH groups (four of eight amides) should form a NH···S or NH···O hydrogen bond in the crystal structure. This result is consistent with the structure determined by our X-ray crystallographic study.

The hydrogen bonding is also expected even in polar solvents such as DMF, DMSO, and CH_3CN. Electrochemical measurement of **2** showed that the Mo^{IV}/Mo^{V} redox potential was

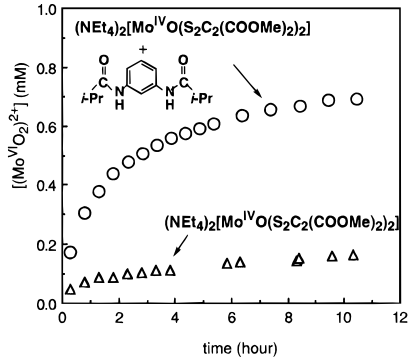

Figure 12. ^{1}H NMR time conversion curve of the Me_3NO reduction by $(NEt_4)_2[Mo^{IV}O\{S_2C_2(COOMe)_2\}_2]$ (**3**) in the presence of $(i\text{-PrCONH})_2C_6H_4$ (**1**) (○) and in the absence of **1** (△) in DMSO-d_6 at 27 °C.

Table 4. Cyclic Voltammetry Data for $(Mo^{IV}O)^{2+}$ Dithiolene Complexes $(NEt_4)_2[Mo^{IV}O\{S_2C_2(COOMe)_2\}_2]$ (**3**) and $(PPh_4)_2[Mo^{IV}O\{S_2C_2(CN)_2\}_2]$ (**4**) in the Presence of Multiamide Additive ($(i\text{-PrCONH})_2C_6H_4$ (**1**) (Conditions: Scan Rate, 100 mV/s; [Mo] = 7 mM; [n-Bu_4NClO_4] = 0.1 M, at 21 °C)

	E_{pc} (mV)	E_{pa} (mV)	ΔE_p (mV)	$E_{1/2}$ (mV)	$I_{pc}I_{pa}^{-1}$
3 + **1** in CH_2Cl_2	−105	+63	168	−21	0.82
3 in CH_2Cl_2	−134	+99	233	−18	0.90
3 + **1** in DMSO	+85	−8	93	+39	1.01
3 in DMSO	+55	−49	104	+3	1.02
4 + **1** in CH_3CN	+536	+437	99	+487	0.89
4 in CH_3CN	+585	+413	172	+499	0.86

Table 5. Initial Rate Constants for the Me_3NO Reduction by $(NEt_4)_2[Mo^{IV}O\{S_2C_2(COOMe)_2\}_2]$ (**3**) and Pseudo-First Order Rate Constants for the Me_3NO Reduction by $(PPh_4)_2[Mo^{IV}O\{S_2C_2(CN)_2\}_2]$ (**4**), in the Presence of Additive $(i\text{-PrCONH})_2C_6H_4$ (**1**) ([Mo] = 7 mM, [Me_3NO] = 10 mM at 27 °C)

	k_{obs}	yield (%) of Mo(VI) complex (10 h after)
3 + **1** (1:1) in DMSO-d_6[a]	7.7×10^{-5} mM s^{-1}	70
3 + **1** (1:0.6)in DMSO-d_6[a]	6.6×10^{-5} mM s^{-1}	70
3 in DMSO-d_6[a]	1.3×10^{-5} mM s^{-1}	15
4 + **1** (1:1) in DMF[b]	$(9.0 \pm 0.3) \times 10^{-5}$ s^{-1}	
4 in DMF[b]	$(11.6 \pm 0.5) \times 10^{-5}$ s^{-1}	

[a] The yield of $(NEt_4)_2[Mo^{VI}O_2\{S_2C_2(COOMe)_2\}_2]$ (**8**) was determined by ^{1}H NMR. Each initial reaction rate was derived from the yield during 15−45 min from the start of the reaction ($k_{obs} = -d[Mo^{IV}]/dt$). [b] Determined by UV/vis spectra. Data were analyzed by pseudo-first order kinetics, $d[Mo^{IV}]/dt = -k_{obs}[Mo^{IV}]$. [c] All errors are random errors estimated at the 99% confidence level (2.5σ).

significantly shifted from that of **3** (Δ(**2**−**3**) = +0.52 V). The positive shift of the redox potential has already been observed in many benzenethiolate complexes as a consequence of NH···S hydrogen bond formation.[14,15a] Thus, even in solution, complex **2** retains NH···S and NH···O interactions.

Me_3NO Reduction by Complex 2. The spectroscopic change in the reaction of **2** with 10 equiv of Me_3NO was recorded by UV/vis spectra. Figure 16 shows the UV/vis spectra of **2** (solid line) in DMF. After Me_3NO was added to the DMF solution, the absorbance increased and the color immediately changed to dark brown within 1 s. The spectra shown in Figure 16 (dashed line) was taken 10 s after the addition of Me_3NO. The reaction system was checked every 1 h until 12 h and did not show any spectral changes. The final spectrum has the same pattern of absorption bands of **2** (formation of $[Mo^{VI}O_2\{S_2C_2(CONH_2)_2\}_2]^{2-}$ (**13**): 291, 339, 435, and 506 nm) as observed in the reaction of **3** (formation of **8**: 290, 360, 417, and

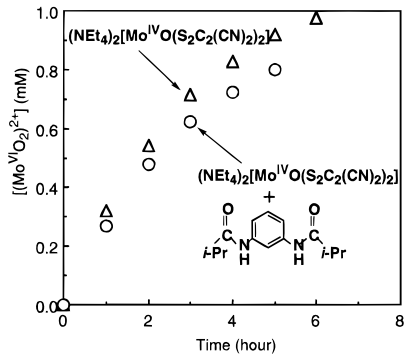

Figure 13. ^{1}H NMR time conversion curve of the Me_3NO reduction by $(NEt_4)_2[Mo^{IV}O\{S_2C_2(CN)_2\}_2]$ (**4**) in the presence of $(i\text{-PrCONH})_2C_6H_4$ (**1**) (○) and in the absence of **1** (△) in DMF at 27 °C.

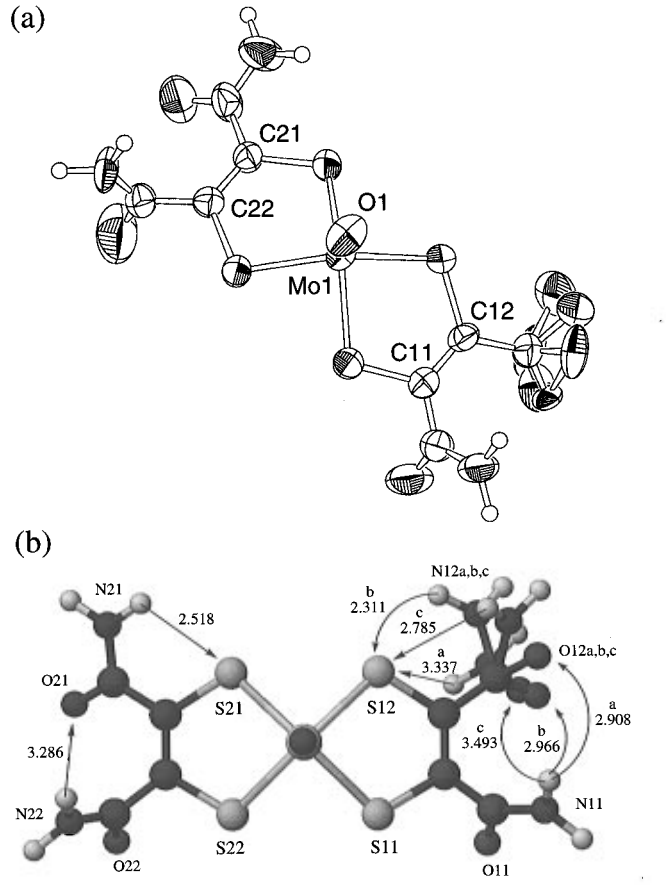

Figure 14. (a) ORTEP drawing of the anion part of $(n\text{-Pr}_4N)_2[Mo^{IV}O\{S_2C_2(CONH_2)_2\}_2]\cdot 0.5(i\text{-PrOH})\cdot$DMF (**2**). (b) Distances (Å) for NH···S and NH···O interactions.

530 nm).[10,19] Thus, we concluded that the reaction proceeded by a simple Me_3NO reduction as shown in eq 4.

$$[Mo^{IV}O\{S_2C_2(CONH_2)_2\}_2]^{2-}\ (\mathbf{2}) + Me_3NO \rightarrow [Mo^{VI}O_2\{S_2C_2(CONH_2)_2\}_2]^{2-}\ (\mathbf{13}) + Me_3N \quad (4)$$

The formation of $[Mo^{VI}O_2\{S_2C_2(CONH_2)_2\}_2]^{2-}$ (**13**) was detected by Raman spectroscopy (Figure 17). The sample was prepared from the reaction mixture, where the solvent was removed *in vacuo* immediately. In the spectra, a typical $(Mo^{VI}O_2)^{2+}$ structure was detected by the two bands at 907 and 867 cm^{-1} which were associated with symmetric and antisymmetric Mo^{VI}═O stretchings, respectively. Even with use of three different excitation lines (457.9 and 514.5 nm (resonance condition) and 1024 nm (off-resonance condition)), any Raman signals from $(Mo^{IV}O)^{2+}$ complex **3** were not observed. Therefore, the reaction was essentially completed, and the quantitative formation of **13** in this reaction condition was shown.

Table 6. Crystal and Refinement Data for $(n\text{-Pr}_4N)_2[Mo^{IV}O\{S_2C_2(CONH_2)_2\}_2]\cdot 0.5(i\text{-PrOH})\cdot$DMF (**2**)

chem formula	$C_{36.5}H_{75}O_{6.5}N_7S_4Mo$	F(000)	4008.00
		radiation	Mo Kα
MW	940.24	μ(Mo Kα), cm^{-1}	4.76
cryst color	dark brown	temp, °C	23
cryst shape	prismatic	scan speed, deg min^{-1}	16
cryst syst	tetragonal	2θ range, deg	6−60
space group	$P4_32_12$ (No. 96) or $P4_12_12$ (No. 92)	octants	$+h, +k, +l$
		no. of reflcns	8175
a, Å	17.05(2)	no. of data used	4772
c, Å	34.33(2)	($I_o > 3\sigma(I)$)	
V, Å^3	9973(7)	R	0.052
Z	8	R_w	0.061
d_{calcd}, g cm^{-3}	1.252	goodness of fit	2.00

Table 7. Comparison of R, R_w, and Goodness of Fit (GOF) Values and Bond Lengths (Å)

	R	R_w	GOF	bond length	
		Model 1			
N22 O21 O22 N21	0.052	0.061	2.00	O11−C13	1.234(9)
				O21−C23	1.23(1)
				O22−C24	1.287(9)
				N11−C13	1.33(1)
				N21−C23	1.30(1)
				N22−C24	1.212(10)
		Model 2			
O22 O21 N22 N21	0.056	0.066	2.18	O11−C13	1.224(10)
				O21−C23	1.24(1)
				O22−C24	1.25(1)
				N11−C13	1.32(1)
				N21−C23	1.29(1)
				N22−C24	1.23(1)

We can conclude that the rate constant (k_{obs}) should be larger than 1 s^{-1} as estimated from the fast change of the UV/vis spectrum and the quantitative formation of $(Mo^{VI}O_2)^{2+}$ complex **13**. Therefore, the rate constant of eq 4 is 10^4-10^5 times faster than the other cases of similar reactions of dithiolene complexes **3** and **4**. This enhanced rate probably comes from the presence of primary amide groups on the dithiolene ligands of **13** which can form NH···S and NH···O hydrogen bonds.

The Raman frequencies of $\nu(Mo^{VI}-S)$ and $\nu(Mo^{VI}=O)$ of **13** were shifted to higher wavenumbers (24 and 22−37 cm^{-1}, respectively) than the other $(Mo^{VI}O_2)^{2+}$ complexes **6** and **8**, as shown in Table 10. These observed shifts indicate the strengthening of both $Mo^{VI}-S$ and $Mo^{VI}=O$ bondings, which probably come from the primary amide groups and the NH···S hydrogen bond formation. Actually, the increased strength of Mo−S bonding by the NH···S hydrogen bond has been observed in Mo(V) and Mo(IV) acylaminobenzenethiolato complexes.[15a] Thus, we can conclude that the presence of primary amide groups in **2** caused the product stabilization of $(Mo^{VI}O_2)^{2+}$ complex **13** and highly accelerated the Me_3NO reduction by **2**.

Discussion

Some of the O-atom transfer enzymes, such as molybdenum and tungsten oxidoreductases, and cytchrome P-450, have been postulated to have a *trans* oxo−metal−thiolate structure as one of the active states. On the other hand, from the model studies,[10,11,19,20,32,33,36−39] the authors have revealed that the a *trans* oxo−metal−thiolate structure is suitable for activation or stabilization of oxo−metal species through the π- and σ-interactions of metal d and ligand p orbitals. To regulate an oxo−metal reactiviy, we have studied multiamide switches which can form NH···S hydrogen bonds.

In the crystal structures of dioxotungsten(VI) and dioxomolybdenum(VI) tetrathiolato complexes,[19,21,37,39] two elongated

Table 8. Comparison of Structural Parameters (Bond Lengths, Å, Bond Angles, deg) for the Anion Part of $(n\text{-Pr}_4N)_2[Mo^{IV}O\{S_2C_2(CONH_2)\}_2]\cdot 0.5(i\text{-PrOH})\cdot$DMF (**2**), $(NEt_4)_2[Mo^{IV}O\{S_2C_2(COOMe)\}_2]$ (**3**), and $(PPh_4)_2[Mo^{IV}O\{S_2C_2(CN)\}_2]$ (**4**)[a]

	2	**3**	**4**
Mo═O			
(mean)	1.682(6)	1.686(6)	1.69(1)
Mo−S			
(mean)	2.376(7)	2.380(4)	2.406(23)
range	2.368(3)−2.384(3)	2.590 (3)−2.604(3)	2.400(3)−2.427(3)
S−C			
(mean)	1.779(11)	1.758(9)	1.73(2)
range	1.763(9)−1.786(9)	1.747(9)−1.769(8)	1.72(1)−1.75(1)
C═C			
(mean)	1.34(0)	1.32(1)	1.36(1)
range	1.34(1), 1.34(1)	1.33(1), 1.31(1)	
C−C			
(mean)	1.475(49)	1.47(2)	1.48(2)
range	1.53(1)−1.41(1)	1.45(1)−1.50(2)	1.47(1)−1.49(1)
∠(Mo−S−C)			
(mean)	107.7(4)	106.1(3)	103.2(11)
range	107.4(3)−108.3(3)	105.8−106.4	102.4(3)−105.0(4)
∠(O−Mo−S)			
(mean)	108.8(8)	108.9(5)	107.0(9)
range	109.5(2)−107.7(2)	108.2(2)−110.0(2)	105.9(5)−108.0(5)
∠(S−Mo−S)(intraligand)			
mean	82.8(4)	83.1(1)	83.3(15)
range	83.0(1), 82.5(1)	83.1(1), 83.0(1)	82.5(1), 84.0(1)
∠(S-Mo-S)(interligand)			
mean	142.44(68)	142.1(2)	145.96(22)
range	141.96(9), 142.92(9)	140.7(1), 143.5(1)	145.85(7), 146.07(8)
mean	85.4(1)	84.8(7)	86.9(4)
range	84.4(1), 86.3(1)	84.3(1), 85.3(1)	87.1(1), 86.7(1)

[a] The number in the parentheses represents the individual standard deviation or the standard deviations from the mean, σ. $\sigma = (\sum_{i=1}^{N}(x_i - x_{mean})^2/N(N-1))^{1/2}$.

Table 9. Raman (IR) Bands (Solid State, KBr Disk; cm^{-1}) of ν(C═C), ν(W═O), and ν(W−S), UV/Vis Absorption Maxima (in DMF; λ, nm (ϵ, M^{-1} cm^{-1})) and Redox Potentials (in CH_3CN; V vs SCE) of $(n\text{-Pr}_4N)_2[Mo^{IV}O\{S_2C_2(CONH_2)\}_2]\cdot 0.5(i\text{-PrOH})$

	ν(C═C)	ν(WdO)	ν(W−S)	λ_{max} (ϵ)	redox potential
2	1540 (1530)	948 (937)	367	337 (9100) 377 (sh, 2600) 422 (sh, 900) 535 (180)	−0.15
3	1535 (1530)	905 (907)	365	358 (9000) 387 (sh, 2800) 444 (sh, 7100) 563 (340)	−0.67
4	1491 (1495)	948 (937)	344	295 (sh, 3000) 334 (5900) 356 (sh, 7000) 387 (sh, 4800) 497 (300) 606 (150)	+0.47

metal−thiolate bond lengths were first discovered for the oxo−*trans*-thiolate ligands. The bond elongation is due to the mutual *trans* influence between the strong π- and σ-donor ligands, oxo and thiolate. Similar *trans* influence was also observed in the lower frequency shift of $\nu(M^{VI}{=}O)$ (M = W and Mo) wavenumbers. The electronic state of the thiolato activated oxo−metal bond features was already analyzed by resonance Raman spectroscopy and molecular orbital calculations.[10]

In addition to the oxo activation, the oxo−metal−thiolato structure must be stabilized sometime during the oxo acception process in the enzyme catalytic cycle. Therefore, we tried to introduce molecular devices into the model systems. For regulation the reactivity of oxo ligands, two principles are to be utilized. One is the extended π-conjugation connected to thiolate, e.g., 1,2-benzenedithiolate and their derivatives to enhance the electron delocalization effect in modulation of the *trans* influence.[37,38] Actually, the enzyme active site has π-conjugated chelating dithiolate, i.e., pterin cofactor, which has a unique dithiolene structure. The second is NH···S hydrogen bonding. Generally, NH···S hydrogen bonds have been found for many of the thiolate ligands at electron transfer protein active sites, such as iron−sulfur proteins and blue copper

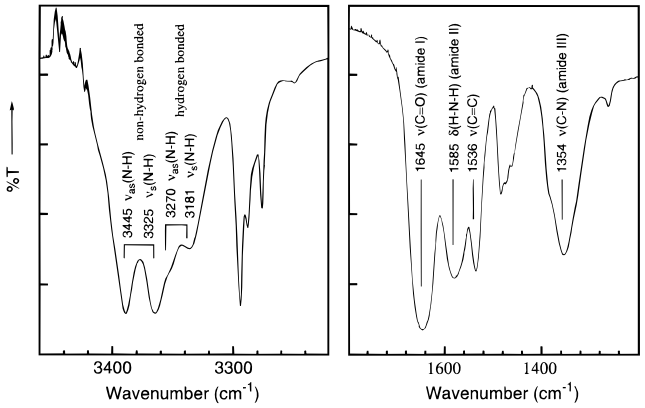

Figure 15. ν(N−H) and amide region of IR spectra for $(n\text{-Pr}_4N)_2[Mo^{IV}O\{S_2C_2(CONH_2)_2\}_2]\cdot 0.5(i\text{-PrOH})\cdot$DMF (**2**). In solid state, KBr disk was used.

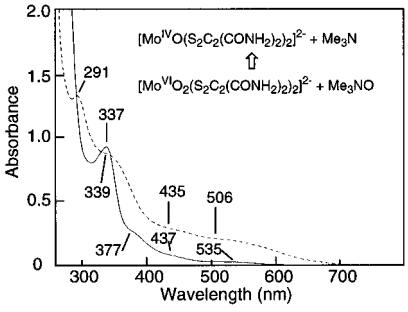

Figure 16. UV/vis spectral change in the oxidation of $(n\text{-Pr}_4N)_2[Mo^{IV}O\{S_2C_2(CONH_2)_2\}_2]\cdot 0.5(i\text{-PrOH})\cdot$DMF (**2**) with Me_3NO: (—) **2**; (- -) **2** + 10Me_3NO (measured after 10 s.) Reaction conditions: [Mo] = 1 mM; [Me_3NO] = 10 mM in DMF at 27 °C.

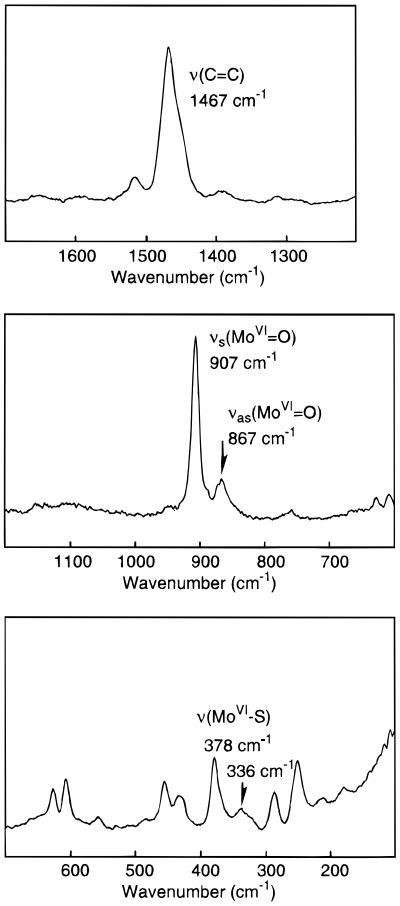

Figure 17. Raman spectra of the ν(Mo═O) and ν(C═C) regions for the *in situ* formed $[Mo^{VI}O_2\{S_2C_2(CONH_2)_2\}_2]^{2-}$ (**13**) complex. Conditions: solid state; 50 mW laser power; 5 cm^{-1} slit width; 60 s accumulation time.

Table 10. Comparison of the Raman Bands (cm^{-1}) of $[Mo^{VI}O_2(dithiolene)_2]^{2-}$ Complexes[29]

dithiolene ligands	ν(Mo^{VI}−S)	ν(Mo^{VI}═O)	ν(C═C)
$S_2C_2(CONH_2)_2$ (**13**)	378	907 867	1468
$S_2C_2(COOMe)_2$ (**8**)		870 838	1503
$S_2C_2(CN)_2$ (**6**)	354	885 851	1472

proteins where the NH···S hydrogen bond regulates the metal−thiolato bonding nature.[12−18] In the case of tungsten and molybdenum oxidoreductases,[6] we can expect hydrogen bonds between the thiolate and the NH of pterin ring of tungstopterin cofactor.[11] Therefore, we have examined the presence of intermolecular and intramolecular NH···S hydrogen bonds in their model complexes. An acceleration of the O-atom acceptance and the stabilization of oxo−metal bonds were observed in the higher rate constant and the high-frequency-shifted Raman bands, respectively. A diamide−dithiolene $(Mo^{VI}O_2)^{2+}$ complex, **13**, which is expected to have NH···S hydrogen bonds, shows $\nu(Mo^{VI}═O)$ at 907 (s) and 897 (as) cm^{-1}. In the case of the ester having $(Mo^{VI}O_2)^{2+}$ complex **8**, which has no NH···S hydrogen bond, $\nu(Mo^{VI}═O)$ bands were observed at 870 (s) and 838 (as) cm^{-1}. Thus, we have concluded that the NH···S hydrogen bonds strengthen Mo═O bonds and stabilize oxo ligands through the *trans* O═Mo^{VI}− thiolate structure. With use of the regulation device, e.g., the NH···S hydrogen bond, the oxo ligand is stabilized at the resting state and then activated upon removal of these effects.

In this paper, we have revealed that the multiamide switches can modulate the reactivity of oxo−metal species by hydrogen bonding through the *trans* oxo−metal−sulfur structure. Generally, enhanced covalency is expected at the metal−thiolato bond in the cases of Mo, W, and Fe, which are found in most of the O-atom transfer enzyme active sites. Therefore, as a consequence of dπ−pπ interaction at the oxo−metal−sulfur bond, the oxo ligand is expected to be activated or stabilized in those enzyme active sites with the controlling device, i.e., the hydrogen bonds. This is one of the answers to the question, "Why is the thiolate ligand utilized in the oxo-transfer enzyme active site?"

Conclusion

By use of the specially designed multiamide additive **1**, a specific association with dithiolene complexes **3**, **4**, and **6** has been studied. Molecular recognition was observed between **1** and complexes **3**, **4**, and **6**. In the CD_2Cl_2 solution of the association system, **1** has suitable conformation for the binding to each complex at the thiolato ligands with varying conformational angles of the amide arms. For Me_3NO reduction, the reaction of Mo(IV) complex **3** was accelerated to form Mo(VI) complex **8** and Me_3N. The reaction acceleration by the NH···S hydogen bond was further supported by the same Me_3NO reduction system using the diamide−dithiolene Mo(IV) complex **2**. Thus, we have constructed a reactivity modulating system with use of the designed additive switch where the formation of a hydrogen bond can provide a regulatory system. This result indicates the importance of specific hydrogen bonds in native metalloenzymes for the switching of their reactivity.

Acknowledgment. We are grateful for financial supports by JSPS Fellowships (for H.O.; Grant No. 1278 (1993−1995), Grant No. 2947 (1995−1998)) and by a Grant-in-Aid for Specially Promoted Research from the Ministry of Education, Science and Culture (for A.N.; Grant No. 06101004).

Supporting Information Available: Text describing the experimental procedures of the crystallographic study (2 pages). Ordering information is given on any current masthead page.

IC951277G